Memoirs of the Faculty of Engineering, Nagoya University
Vol. 38, No. 2 (1986)

# EFFECTS OF POLYMER-POLYMER INTERFACES ON ELECTRICAL PROPERTIES OF INSULATING COMPOSITES

MASAYUKI IEDA, GUO-XIONG CAI,
YASUO SUZUOKI and TERUYOSHI MIZUTANI

*Department of Electrical Engineering*

(Received October 31, 1986)

**Abstract**

As most of Practical insulation systems are composed of several insulating materials, semiconductors and conductors, interfacial phenomena are considered to play an important role. In order to clarify the effects of interface, thermally stimulated current (TSC), conduction current and dielectric breakdown measurements were carried out on the composite of EVA (ethylene-vinyl acetate copolymer) and PE (polyethylene) and also on other combination of polymer materials.

The TSC and conduction current in EVA-PE showed remarkable dependence on the polarity of the applied voltage, which cannot be explained by the simple Maxwell-Wagner model. This is explained as follows. Positive carriers are easily injected into EVA from the Au anode. Some of them are trapped at the EVA-PE interface and give rise to a new interfacial TSC peak. Most of the positive carriers can pass through the interface and move in the PE layer, increasing the conduction current in PE by about two orders of magnitude. The conduction current measurements also revealed that the existence of some polar groups at the metal-PE interface enhances carrier injection into PE.

Methods were proposed for analyzing the internal fields in the composite system to which the simple Maxwell-Wagner model could not be applied. The internal field under very high field near dielectric breakdown strength was estimated from the breakdown strength of the composite. The internal field under lower fields was estimated by the separation method developed here. It was revealed that the ratio of internal fields of PE and EVA layers dependes on the polarity, field and temperature. The latter method also clarified that the positive

carriers trapped at the EVA-PE interface were located on the EVA side.

Other combinations of polymers also showed the same polarity dependence as EVA-PE, suggesting that EVA-PE was not an exceptional case but that similar phenomena also took place in practical insulating composites.

## CONTENTS

1. General Introduction ..... 139
2. TSC from Laminated Polymeric Dielectrics ..... 141
2. 1. Introduction ..... 141
2. 2. Experimental Method and Specimens ..... 142
2. 3. TSC from Ethylene-Vinyl Acetate Copolymer (EVA) and Polyethylene (PE) ..... 144
2. 4. Influence of Interface on TSC Spectra ..... 145
2. 5. EVA-PE Two-Layer Film with Metal at Interface ..... 148
2. 6. Bias TSC of EVA-PE ..... 150
2. 7. TSC from PE-EVA-PE and EVA-PE-EVA Three Layer Films ..... 150
2. 8. Model of EVA-PE Laminate Films ..... 151
2. 9. Dependence of TSC Spectra on Electrode Metal ..... 152
2. 10. Dependence of TSC Spectra on Poling Temperature ..... 152
3. Electrical Conduction of EVA, PE and Their Composites ..... 153
3. 1. Introduction ..... 153
3. 2. Experimental ..... 153
3. 3. Electrical Conduction of PE ..... 153
3. 4. Electrical Conduction of EVA ..... 154
3. 5. Electrical Conduction of Laminate Films ..... 156
3. 6. Model of Conduction of EVA-PE Laminate Films ..... 159
3. 7. Conduction Current of EVA with Semi-Conducting Layer ..... 159
3. 8. Effects of Polar Groups on Electrical Conduction in Polyethylene ..... 161
4. Discharge Currents in EVA Film and EVA-PE Laminate Films ..... 162
4. 1. Introduction ..... 162
4. 2. DC Discharge Currents of EVA-PE ..... 163
4. 2. 1. Released Charges Calculated from $P_4$ TSC Peak and Discharge Current ..... 163
4. 2. 2. Released Charges Calculated from $P_5$ TSC Peak and Discharge Current. ..... 164
4. 3. AC Discharge Current of EVA-PE and EVA ..... 165
5. Breakdown Strength of EVA-PE Laminate Films ..... 168
5. 1. Introduction ..... 168
5. 2. DC Breakdown Strength ..... 168
5. 3. Impulse Breakdown Strength ..... 171
6. Evaluation of Internal Electric Field by Separation Method ..... 172
6. 1. Introduction ..... 172
6. 2. Separation Method ..... 172
6. 3. Accuracy of Separation Method ..... 173
6. 4. Internal Field Evaluation from Dipolar TSC Peak ..... 175
6. 5. Location of Charges Responsible for Interfacial TSC Peak in EVA(+)-PE(−) ..... 177
7. TSC and Conduction Current of Other Combinations of Polymers ..... 178
7. 1. Introduction ..... 178

7. 2. TSC and Conduction Currents of EVA-HDPE, EVA-PP, EVA-FEP and EVA-PET ..... 178
8. Conclusion ..... 180
Acknowledgements ..... 181
References ..... 181

## 1. General Introduction

For the increasing demand for electric power and for the improvement of the efficiency of electric power transmission, AC and DC UHV (ultra high voltage) power transmission lines have been developed nowadays. The application of UHV transmission system highlights the problem of high voltage insulation. On the other hand, in the field of microelectronics, the increasing density of devices in LSI also needs high quality insulation. Although the applied voltage is low in electronic devices the electric field is high in the insulating layers.

The common demand on insulation in power transmission systems and micro electronic devices is to withstand high electric field. This has gradually changed the concept of "high voltage techniques" to "high electric field techniques". For the purpose of high field insulation, polymeric insulating materials are gradually widely used in the field of power engineering, since they have more advantages than traditional insulating materials.

In order to make better insulation design, it is necessary to understand various electrical phenomena in insulating materials. The basic electrical properties of insulating materials are summarized as follows:

(a) electrical insulation properties
  (i) electrical conduction
  (ii) dielectric breakdown
(b) dielectric properties
  (i) electrical polarization
  (ii) dielectric loss

Great efforts have been made to understand the electrical conduction mechanisms and space charge accumulation in polymeric insulating materials. If it is possible to completely understand the relationship between microscopic molecular structures and macroscopic electrical properties of polymeric insulating materials, it is of benefit not only in the field of insulation design, but also in the field of material design. However, the electrical conduction, breakdown and aging behaviors are very much complicated and sometimes they are not determined by one mechanism only. The mechanisms of conduction, breakdown and aging depend upon the environmental conditions such as temperature and applied voltage. These facts make it more difficult to handle the problems.

In addition to electrical insulation and dielectric properties, mechanical properties play an important role in insulation design. It is necessary for insulating materials to have enough mechanical strength.

In the field of electrical insulation, in addition to the development of new materials, there is another approach to satisfy various requirements. This is the application of the composite insulation which combine favorable properties of several materials.

From a wide point of view, even in a single insulating material such as polyethylene, the crystalline and amorphous parts form a kind of composite. From an engineering point of view, one of the advantages of applying composite insulation systems is to decrease the cost. Fillers added in epoxy resin not only improve insulating properties, but also decrease the cost. For the reasons mentioned above the investigation of electrical properties of insulating composites is very important. In the study of a composite system the properties of its interfaces are considered to be very important.

When a composite insulating system is analyzed, the Maxwell-Wagner model[1] is traditionally applied. The basic idea of the Maxwell-Wagner model is to consider the conductivity and the permittivity of each insulating material and to calculate the resistance and the capacitance of the composite by means of circuit analysis. Consider, for example, a plane-parallel dielectric slab consisting of two layers of different materials of thickness $\delta_1$ and $\delta_2$, dielectric constants $\varepsilon_1$ and $\varepsilon_2$ and conductivities $\sigma_1$ and $\sigma_2$, respectively. Then, the conduction current density in each layer is given by

$$i_{1c}=\sigma_1 F_1 \tag{1}$$

$$i_{2c}=\sigma_2 F_2 \tag{2}$$

where $i_{1c}$ and $i_{2c}$ are the conduction current densities in layers 1 and 2, respectively, and $F_1$ and $F_2$ are the electric fields in layers 1 and 2, respectively. The displacement current density in each layer is given by

$$i_{1d}=\varepsilon_1 \partial F_1/\partial t \tag{3}$$

$$i_{2d}=\varepsilon_2 \partial F_2/\partial t. \tag{4}$$

The total current density $i$ is given by

$$\begin{aligned} i &= i_{1c}+i_{1d}=i_{2c}+i_{2d} \\ &= \sigma_1 F_1+\varepsilon_1 \partial F_1/\partial t=\sigma_2 F_2+\varepsilon_2 \partial F_2/\partial t. \end{aligned} \tag{5}$$

The total applied voltage $V$ is given by

$$V=\delta_1 F_1+\delta_2 F_2. \tag{6}$$

From equations (5) and (6), one obtains

$$F_1=[V\sigma_2/(\sigma_1\delta_2+\sigma_2\delta_1)]+C\exp(-t/\tau) \tag{7}$$

where $C$ is a constant and

$$\tau=(\delta_2\varepsilon_1+\delta_1\varepsilon_2)/(\delta_2\sigma_1+\delta_1\sigma_2) \tag{8}$$

For the case of step-like voltage application, the initial condition

$$F_1(t=0)=(\varepsilon_2 V)/(\varepsilon_2\delta_1+\varepsilon_1\delta_2) \tag{9}$$

gives the constant $C$ in equation (7). The internal field $F_1$ is then given by the following expression,

$$F_1=[V\sigma_2/(\sigma_1\delta_2+\sigma_2\delta_1)]+[(\varepsilon_2V)/(\varepsilon_2\delta_1+\varepsilon_1\delta_2)$$
$$-(V\sigma_2)/(\sigma_1\delta_2+\sigma_2\delta_1)]\exp(-t/\tau). \quad (10)$$

From equations (1) and (2), the conduction currents in layers 1 and 2 are calculated. The amount of charges accumulated at the interface is expressed by

$$Q=\int_0^\infty (i_{1c}-i_{2c})dt. \quad (11)$$

Some reports proved that Maxwell-Wagner model could explain the TSC in epoxy-mica insulating composites[2,3]. However, the Maxwell-Wagner model is inapplicable to certain cases, e.g. the polyethylene (PE) and ethylene-vinyl acetate copolymer (EVA) composite system, as will be discussed in this report. Therefore, the EVA-PE laminate film is a good system to study interfacial phenomena in insulating composites. There are some applications of EVA-PE composites. This has been applied to a proto-type cable to decrease water trees by Chubu Electric Power Company Inc. and Tatsuta Cable Co., Ltd.[4~6].

## 2. TSC from Laminated Polymeric Dielectrics

### *2. 1. Introduction*

In order to clarify transport phenomena and other physical properties of dielectrics, many investigations have been carried out by means of thermal stimulation. There are several methods for investigating dielectric materials by thermal stimulation, such as thermally stimulated current (TSC), open TSC and thermally stimulated surface potential (TSSP). In addition, X-ray or high-energy electron beam has been also used[7~10] to study TSC due to carrier traps in dielectrics.

A TSC results not only from carrier detrapping, but also from depolarization of dipoles. Dipolar TSC has been well analyzed theoretically[11], but there is no complete analysis on behaviours of trapped charges and mobile ions in TSC experiments because of the complexity of the phenomena[12].

The authors mainly deal with interfacial trapped carriers in this chapter. For the purpose of studying interfacial trapped carriers, low density polyethylene (PE) and ethylene-vinyl acetate copolymer (EVA) films were used.

Polyethylene is one of the widely-used polymeric materials. It is used not only in the field of electrical insulation, but also in our daily life, since it is easy to process and also has an advantage of no toxic gases being produced while burnt. In the field of UHV insulation system polyethylene is used in XLPE (cross linked polyethylene) cables. In Japan, 275kV XLPE cables are successfully used, and 500kV XLPE cables are under development. From engineering point of view, the study of the carrier transport and generation in polyethylene has crucial importance.

In order to study the polymer-polymer interface with polyethylene, a polymeric material which is similar in chemical structure to polyethylene is desirable as a counterpart. Ethylene-vinyl acetate copolymer meets this requirement and it also has physical properties similar to polyethylene when the vinyl-acetate content is lower than 7 %[13]. There are many reports concerning the physical and electrical properties of EVA[14,15]. The main difference between EVA and PE is that EVA

has more amorphous parts[15] and higher permittivity than PE. It seems that EVA and PE provide preferable combination to study the polymer-polymer interface.

In this chapter the TSC spectra of EVA, PE and their composites are mainly discussed.

### *2. 2. Experimental Method and Specimens*

The TSC experiments were carried out in a vacuum vessel. The block diagram of the instrumental arrangement is shown in Fig. 1. The pressure inside the vessel was held around 0.1 Pa by a rotary vacuum pump. The temperature and the temperature rising rate were controlled by a temperature control unit. Currents were measured by a vibrating reed electrometer (VRE) (Takeda Riken TR-84M).

Two kinds of methods were used to record the data. One is illustrated in Fig. 1. The analog output signal from the VRE is recorded by a pen recorder. The other is digital data acquisition shown in Fig. 2. Digital data from the A/D converter connected to the VRE are transferred to a computer (NEC PC-8001 and its expansion unit PC-8011) via a GP-IB (IEEE-488) data bus and a resultant TSC spectra is plotted by a pen recorder or a X-Y plotter. The TSC measurement is controlled by a control program, which has two main functions. It controls the input control unit to input temperature signal from a thermocouple. The temperature signal is compared with the temperature data in the control program. The TSC signal is read just when the temperature reaches a desired temperature. The other main func-

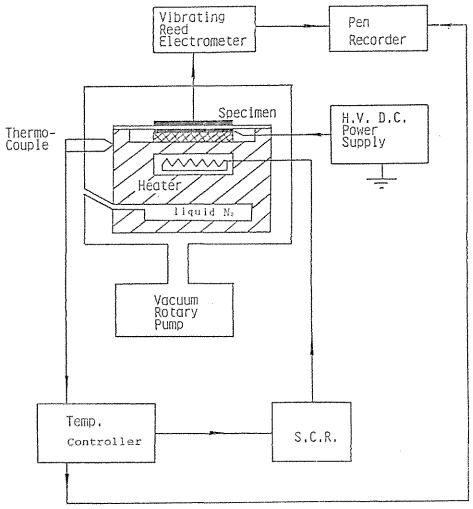


Fig. 1. Schematic diagram of experimental setup.

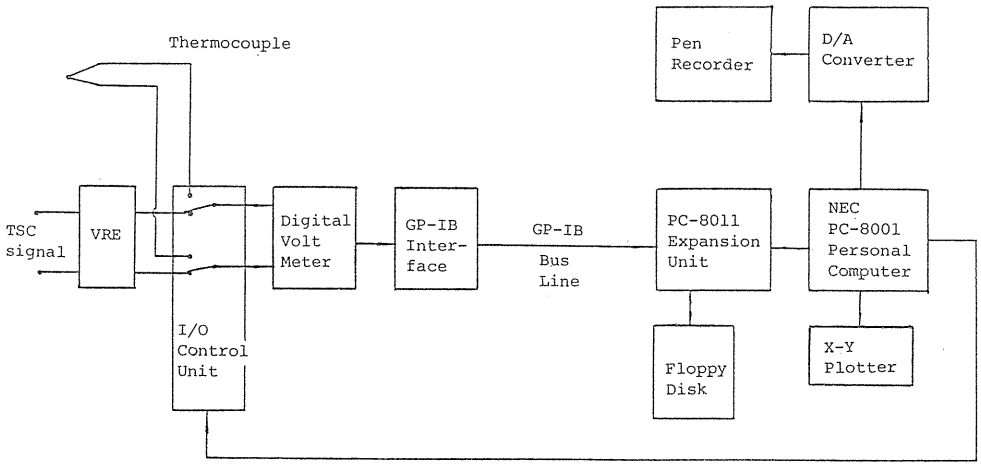


Fig. 2. Block diagram of the computer system for TSC measurement.

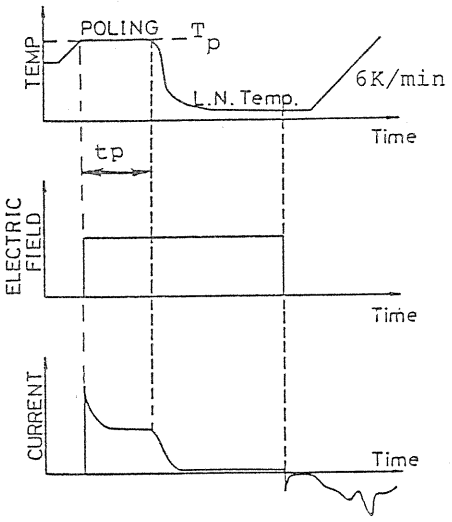


Fig. 3. Experimental procedure for TSC measurements.

tion is to eliminate the noise involved in data. This was done by reading 20 TSC data at each measuring temperature, of which the 5 largest and the 5 smallest are omitted, and by taking an arithmetic mean of the remaining 10 data as a true TSC.

The procedure for TSC measurements is shown in Fig. 3. At a certain temperature $T_p$, a poling electric field is applied to a specimen for a poling time tp and then by using liquid nitrogen, the specimen is promptly cooled to about 90K without removing the poling electric field to make an electret. After the specimen is cooled down to about 90 K the poling electric field is removed and the both sides of the specimen is short-circuited. After the transient current becomes negligible, the temperature is raised at a

Table 1. List of specimens used.

| specimen | code | formula (H is abbreviated) | Tm (K) | Xc(%) | d(μm) | wt.% | making process |
|---|---|---|---|---|---|---|---|
| Polyethylene (LDPE) | PE | $(-\dot{C}-\dot{C}-)_n$ | 408 | 82-85 | 30 | - | - |
| Polyethylene (HDPE) | HDPE | | 381 | 43-47 | 30 | - | - |
| Ethylene-Vinyl Acetate Copolymer | EVA | $[(-\dot{C}-\dot{C})_m-\dot{C}(O-C(=O)-)-\dot{C}-]_n$ | 358-370 | 19-35 | 25 | 22 | - |
| Polypropylene | PP | $(-\dot{C}-\dot{C}-)_n$ with $-\dot{C}-$ | 440 | high | 22 | - | - |
| Tetrafluoroethylene Hexafluoropropylene Copolymer | FEP | $[(-\dot{C}(F)-\dot{C}(F)-)_m-\dot{C}(F)-\dot{C}(CF_3)-]_n$ | 560 | 35 | 12.5 | - | - |
| Polyethylene Terephthalate | PET | $(-\dot{C}-\dot{C}-O-C(=O)-C_6H_4-C(=O)-O-)_n$ | 533 | 41 | 25 | - | - |
| EVA-PE(LDPE) | EVA-PE | | - | - | 15+15 | (22) | blown |
| EVA-PE(LDPE) | EVA-PE | | - | - | 25+30 | (22) | hand |
| EVA-PE(HDPE) | EVA-HDPE | | - | - | 25+30 | (22) | hand |
| EVA-PP | EVA-PP | | - | - | 25+22 | (22) | hand |
| EVA-FEP | EVA-FEP | | - | - | 25+12.5 | (22) | hand |
| EVA-PET | EVA-PET | | - | - | 25+25 | (22) | hand |

$T_m$ : Melting temperature ; Xc : Degree of crystallinity ;
$d$ : Thickness ; hand : hand made ; blown : blown-film ;
wt.% : Weight percent of vinyl acetate unit content.

rising rate of 6K/min and the TSC is measured.

The specimens used in the experiments are listed in Table 1. The term "hand made" refers to the two-layer specimens which are made by putting two films together at room temperature, in distinction from the laminate films supplied by Mitsubishi petrochemical Co. Ltd., which are laminated during the blown-film manufacturing process. A blend of polyethylene and ethylene-vinyl acetate copolymer ("BLEND") is also used as a specimen. The total content of vinyl acetate in the blend specimen was 12.5 wt%. Diameters of the electrodes are 30 mm or 20mm, depending on the experiments. Unless otherwise specified the electrodes were evaporated gold.

In this report, hereafter, low density polyethylene is abbreviated to "PE" or "LDPE", while "HDPE" means high density polyethylene.

### 2. 3. *TSC from Ethylene-Vinyl Acetate Copolymer (EVA) and Polyethylene (PE)*

The application of TSC and thermoluminescence (TL) techniques provided a great deal of information about carrier traps in polymeric insulators[16~20]. Figure 4[21] shows the relation among TSC, TL and mechanical loss ($\Lambda_G$) of PE. Here, the TSC was measured under a bias field of 90 kV/cm for a specimen irradiated with X-rays around 90 K under short-circuit condition. The prior X-ray irradiation was carried out in order to fill carrier traps with excited carriers. TSC and TL show several peaks ($C_1$-$C_5$, $L_1$-$L_3$), indicating the abundance of carrier traps. However, TSC without prior X-ray irradiation, i.e. without the contribution of trapped carriers, shows no peaks. Similar curves were also obtained for HDPE[21]. Since polyethylene is non-polar, polyethylene shows virtually no TSC, except for the very small contribution of carriers.

The TSC spectrum of EVA which contains 22% of vinyl acetate is shown in Fig. 5. It shows three TSC peaks, i.e. $P_1$, $P_2$ and $P_3$. The three peaks are closely related to the mechanical relaxations in EVA. The relaxations in EVA were studied by many researchers[22~24]. According to them there are three relaxations, i.e. the $\alpha$ relaxation in crystalline parts (ca. 60℃ at 110Hz), the $\beta$ relaxation due to micro-Brownian motion of main chains in amorphous parts (ca. −20℃ at 110Hz), and the $\gamma$ relaxation due to local motions (ca. −140℃ at 110Hz).

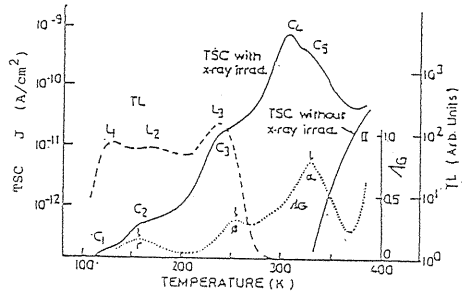


Fig. 4. TSC spectra for LD-PE under a field of 90 kV/cm, together with the TL spectrum and the mechanical loss curve.

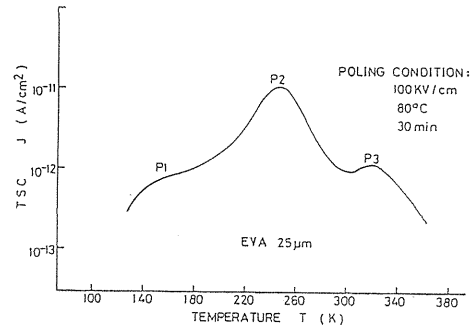


Fig. 5. TSC spectra of EVA single layer film.

The peak temperatures of three TSC peaks in EVA coincide well with those of the $\alpha$, $\beta$, $\gamma$ mechanical relaxations mentioned above. It is concluded that the three TSC peaks are related to dipolar depolarization associated with molecular motions in EVA, i.e.

$P_1$ : local motion in amorphous or crystalline parts[23],

$P_2$ : micro-Brownian motion of main chains in amorphous region[23],

$P_3$ : molecular motion in crystalline parts[23,24].

As shown in Fig. 7, the $P_1$, $P_2$ and $P_3$ TSC peaks have linear dependence on poling electric field. According to the following discussion the linear dependence of the TSC peaks on electric field supports that these are due to dipolar depolarization. On the following assumptions;

(1) The dipole moment is independent of electric field,

(2) interaction energy between the dipoles is negligibly small compared with thermal energy $kT$,

(3) the dipole moment is possible in any direction,

the average dipole moment $\overline{m}$ in the direction of the internal electric field is expressed by

$$\overline{m}=\mu_0 L(a) \quad [25] \tag{12}$$

where $a=\mu_0 F_i/kT$, $\mu_0$ is the Permanent dipole moment, $k$ the Boltzmann's constant, $F_i$ the internal electric field, $T$ the absolute temperature and $L(a)$ the Langevin function. by substituting typical values of $\mu_0=1$ Debye ($3.33\times10^{-30}$cm), $T=300$K, and $F_i=1000$ kV/cm, the value of $a=\mu_0 F_i/kT$ becomes $0.08\ll1$. For $a\ll1$ the Langevin function can be approximated by a linear relation,

$$L(a)\fallingdotseq a/3=\mu_0 F_i/3kT \tag{13}$$

and the average dipole moment can be expressed by

$$\overline{m}=\mu_0^2 F_i/3kT \tag{14}$$

This implies that in the usual electric field range TSC peak due to dipoles has a linear dependence on poling electric field. The $P_1$, $P_2$ and $P_3$ TSC peaks in EVA have linear dependence on poling electric field and their peak temperatures coincide nell with the mechanical relaxation temperatures. Therefore, it is reasonable to conclude that the three TSC peaks in EVA are due to dipoles[26].

### *2. 4. Influence of Interface on TSC Spectra*

In order to study the influence of interface on TSC spectra, TSC from EVA-EVA, PE-PE two layer films were measured as a preliminary experiment.

The TSC spectrum of EVA-EVA two layer specimen is the same as EVA single layer film. The TSC spectrum of PE-PE is very small and it does not show any new peak. In spite of possible oxidized surface layers and gas bubbles located at the EVA-EVA and PE-PE interfaces, their influences on the TSC spectrum are not significant.

To study the EVA-PE interface, especially the carrier accumulation at the interface, TSC's from a two-layer film were observed. As shown in Fig. 6, the TSC spectra in EVA-PE laminated films show a strong dependence on the polarity of the applied poling field. When EVA-PE laminate specimen is polarized with a

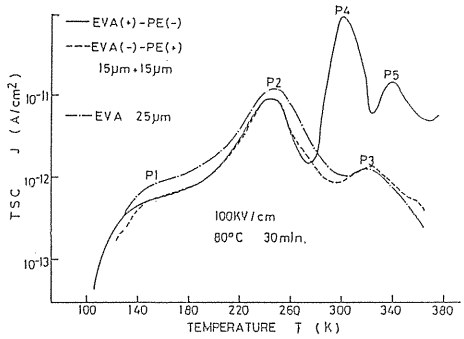


Fig. 6. TSC spectra from EVA-PE laminates and EVA.

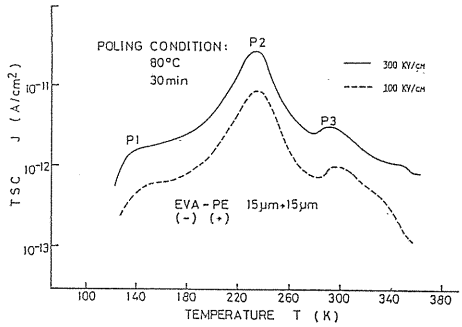


Fig. 7. Electric field dependence of TSC from EVA(−)-PE(+).

negative voltage on the EVA side (EVA(−)-PE(+)), the TSC spectrum is similar to that from a single layer of EVA, and its three peaks coincide with $P_1$, $P_2$ and $P_3$ peaks in EVA. The three TSC peaks increase linearly with poling field, as shown in Fig. 7. These peaks are considered to originate from EVA layer and there is no new peak arising from the interface in the case of EVA(−)-PE(+).

When the polarity of the poling field is reversed (EVA(+)-PE(−)), new TSC peaks, $P_4$ and $P_5$, appear in the high temperature region, while $P_1$ and $P_2$ peaks remain the same. Since $P_4$ peak appears neither in EVA layer nor in PE, it is not reasonable to consider that $P_4$ peak originates from EVA or PE bulk. Since a single EVA layer and a single PE layer have the same metal-polymer interface as the EVA-PE, $P_4$ peak does not originate from the metal-polymer interface (metal-EVA or metal-PE). Therefore, it is reasonable to conclude that $P_4$ peak originates from trapped carriers at the EVA-PE interface.

Another evidence to show that $P_4$ peak is due to trapped carriers is its electric field dependence. Figures 8 and 9 show the dependence of the $P_4$ peak on the poling field. When poling electric field is lower than 75kV/cm, the intensity of $P_4$ peak increases with poling electric field, but above 75kV/cm the intensity decreases with increasing poling electric field. For comparison, $P_2$ TSC peak is also plotted

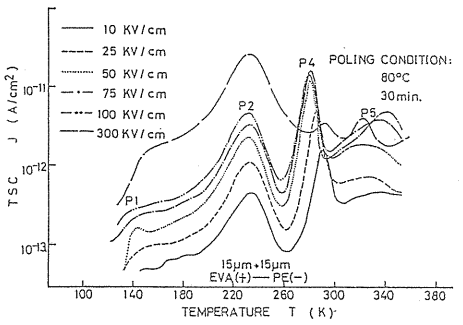


Fig. 8. Electric field dependence of TSC from EVA(+)-PE(−).

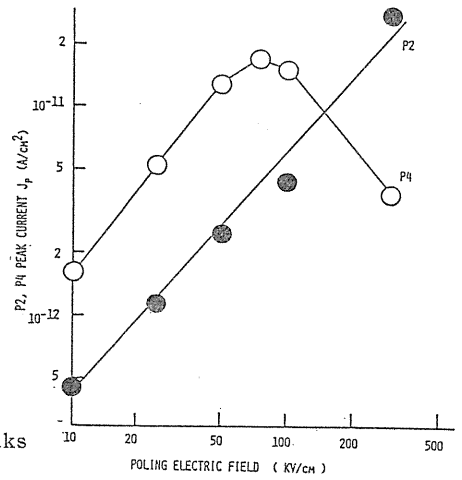


Fig. 9. Intensities of $P_2$ and $P_4$ peaks plotted against poling field.

in Fig. 9, which has linear dependence on electric field. The non-linear dependence of $P_4$ peak is another evidence to show that $P_4$ peak originates not from dipolar depolarization, but from carrier detrapping process.

Possible explanations for the non-linear field dependence of peak $P_4$ are as follows. In the low-field region, the number of carriers trapped at the interface increases with increasing field, for more carriers come into the interfacial region as the field increases. Thus, peak $P_4$ increases with field. In the high-field region, the number of trapped carriers is expected to decrease because of the possible field lowering of the trap depth during the poling process (e.g. the Poole-Frenkel effect[27]). The field lowering of the interfacial barrier is also expected to increase the number of carriers which pass through the interfacial region with the trapping sites responsible for peak $P_4$. Thus peak $P_4$ is expected to decrease with poling field. Assuming the Poole-Frenkel effect for the field reducing of the trap depth and that the amount of charge carriers at the interface under high field can be extrapolated from those under low field, the relative dielectric constant of the interfacial region can be calculated from the dependence of the intensity of peak $P_4$ on the field (Fig. 9). The value obtained was about 2 and was in reasonable accord with the dielectric constants of PE and EVA (ca. 2.3 and 3.1,[28] respectively). The decrease of the temperature of peak $P_4$ shown in Fig. 8, however, is much smaller than expected from the Poole-Frenkel effect.[29] This may be because the internal field during the detrapping process (i.e. during the TSC measurement) is much smaller than that during the poling. It is, therefore, not unreasonable to assume the Poole-Frenkel type field reduction of the trap depth.

The depth of carrier traps responsible for $P_4$ peak can be calculated by the initial rise method. This method estimates activation energy from a slope of the log J versus $(1/T)$ plot of the low temperature tail of a TSC peak[30]. The trap depth for $P_4$ peak was estimated at about 1.5 eV as shown in Fig. 10.

$P_5$ peak is smaller than $P_4$ peak and its behaviour is easily overshadowed by $P_4$ peak. In order to clarify the behaviours of $P_5$ peak, the amount of released charges

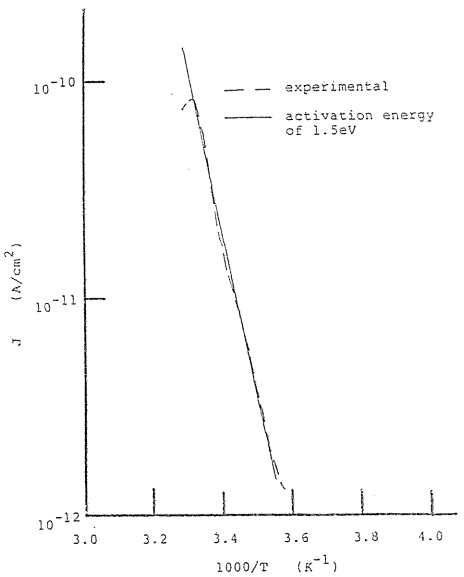


Fig. 10. The activation energy of $P_4$ peak, estimated from the initial rise method.

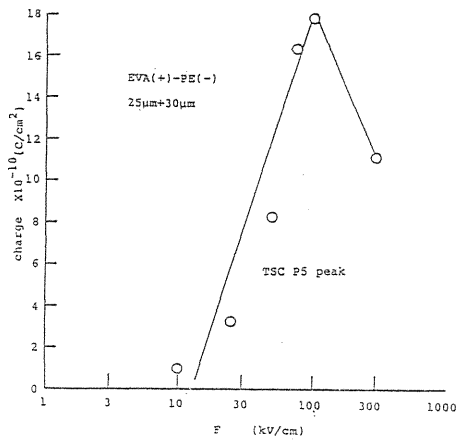


Fig. 11. Charges calculated from $P_5$ TSC peak.

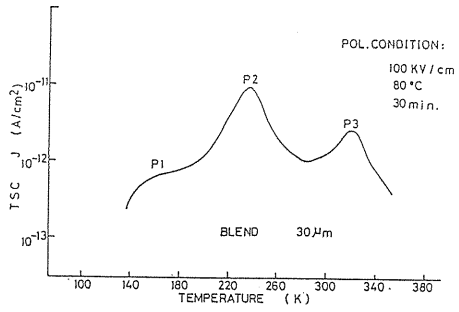


Fig. 12. TSC spectra from EVA-PE blend specimen.

of $P_5$ peak is calculated from the area bound by the $P_5$ peak and the abscissa and its electric field dependence is illustrated in Fig. 11. This shows a non-linear dependence on poling electric field, suggesting that $P_5$ peak originates from carrier detrapping as described in Chapter 4.

The TSC of BLEND (a blend of PE and EVA) in which, unlike the EVA-PE laminates, EVA particles are dispersed is shown in Fig. 12. There is no new peak arising from interfaces. In the case of mica-epoxy resin system, which is also a dispersive system, a TSC peak due to interfacial polarization appears[2,3]. The reason is considered as follows. In the case of EVA-PE system, carriers trapped at EVA-PE interface are greatly dependent upon the amount of positive carriers injected from Au into EVA (cf. Section 2.8.). In a PE and EVA blend specimen, there is less contact area between Au electrode and EVA than in a pure EVA, resulting in less injection to the blend system, and therefore, the interfacial TSC peak does not appear.

### *2. 5. EVA-PE Two Layer Film with Metal at Interface*

As described in Section 2.4., the TSC spectra of EVA-PE show strong polarity dependence, i.e. the interfacial peak appears only when the specimen is polarized with a positive voltage on the EVA side (EVA(+)-PE(−)). This phenomenon can not be explained by the conventional Maxwell-Wagner model[1]. In the Maxwell-Wagner model the internal fields of EVA and PE layers in EVA-PE laminate are determined by the conductivities of single layers of EVA and PE, and do not depend on the polarity of the applied field. The Maxwell-Wagner model is considered to be applicable to the EVA-PE composite system when metal electrode is inserted between EVA and PE (EVA-Metal-PE (EVA-M-PE)). The EVA-M-PE specimen was made by putting EVA and PE films together, each of which had vacuum-deposited gold electrodes on both sides.

Figure 13 shows the TSC spectra of EVA-M-PE. The TSC spectra from EVA (+)-M-PE(−)and EVA(−)-M-PE(+)are essentially the same. However, these TSC spectra are different from EVA(+)-PE (−) and EVA(−)-PE(+) without metal between EVA and PE. The TSC spectra of EVA-M-PE show $P_4'$ peak around 310K instead of $P_4$. The $P_4'$ peak has no polarity dependence and it appears at a temperature higher than $P_4$ peak. The integrated charge of the $P_4'$ peak and the potential of the middle metal electrode coincide well with the values predicted by the Maxwell-Wagner model. These calculated values were obtained by regarding the EVA-PE composite as a series connection of two

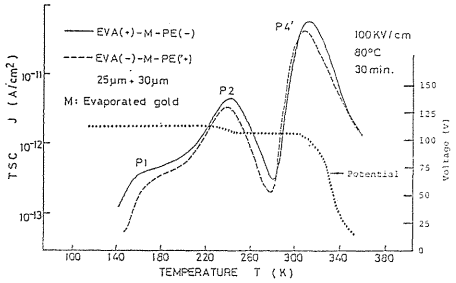


Fig. 13. TSC from EVA-M-PE and the potential of the middle metal electrode.

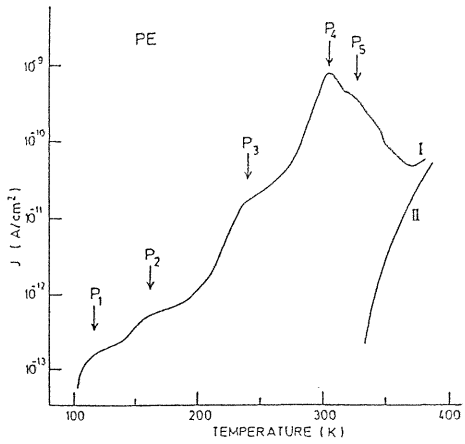


Fig. 14. TSC spectra from PE under a bias voltage of 270V.
Curve I : the first TSC spectrum (with x-ray irradiation at 90K) ;
Curve II : the second TSC spectrum (without x-ray irradiation).

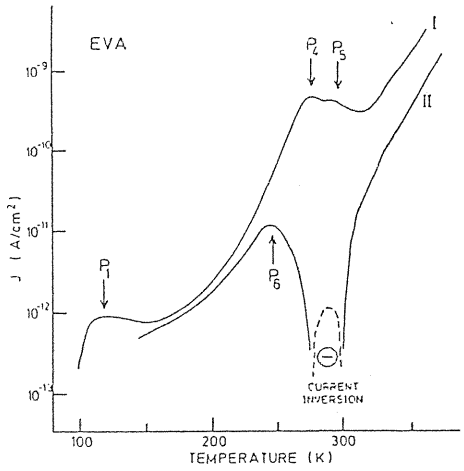


Fig. 15. TSC spectra from EVA under a bias voltage of 270V.
Curve I : the first TSC spectrum (with x-ray irradiation at 90K) ;
Curve II : the second TSC spectrum (without x-ray irradiation).

circuits, each of which consisted of a capacitor and a resister in parallel.

Figures 14 and 15 show X-ray induced TSC spectra in PE and EVA, respectively, where curves I are TSC in the specimen with a prior X-ray irradiation at 90K and curves II are TSC without X-ray irradiation.[31] The second TSC spectra, curves II, were measured under a bias voltage of 270V without the preceding X-ray irradiation and, thus, reflect the dark conductivities of PE and EVA. From the Maxwell-Wagner model the TSC peak is expected to appear at the temperature where the conductivity drastically increases. As shown in Figs. 14 and 15 the conductivities of PE and EVA increase abruptly around 330K and around 300K, respectively. The temperature range of $P_4'$ peak in Fig. 13 coincides well with the abrupt increase of the conductivity of EVA. This also suggests that the Maxwell-Wagner model is applicable to this case. The $P_4'$ peaks are considered to result from the release of charges at the middle metal mainly through the EVA bulk.

The conduction currents of EVA-M-PE do not depend on the polarity of the applied field and are almost as small as that of the single layer of PE (Fig. 24). This is reasonable since (1) the EVA-M-PE system can be regarded as a series connection of M-EVA-M and M-PE-M systems, both of which are independent of each other, and (2) the conduction current in M-EVA-M is larger than that in M-PE-M by about two orders of magnitude at 353K. As exemplified by the EVA-M-PE system, the simple Maxwell-Wagner model is applicable to such a composite system that the nature of each component layer is not influenced by the neighboring layers or the interfaces. However, in the actual composite insulating system, the effects of neighboring layers and interfaces are not always negligible as in the case of the EVA-PE system and these effects should be taken into careful consideration to apply the conventional Maxwell-Wagner model to analyze the composite system.

*2. 6. Bias TSC of EVA-PE*

In Section 2. 4. the TSC spectra of EVA-PE were discussed. When EVA-PE sample is heated to the temperature region of $P_4$ peak after short-circuiting at liquid nitrogen temperature, there are two possible paths for the trapped carriers at the interface to take to dissipate. One is through PE and the other is through EVA. Which path for them to take depends upon the mobilities of the carriers in EVA and PE and upon their exact location in the interfacial region. If these interfacial trapped carriers do not move in only one direction, the current in the external circuit is the difference between those in two directions and the amount of trapped charge cannot be evaluated by integrating the TSC peak current.

In order to clarify the amount of trapped carriers at the interface and to calculate the internal electric fields in EVA and PE, the TSC of EVA(+)-PE(−) under a collecting bias (bias TSC) was measured. Bias TSC is a TSC with a bias voltage applied to the specimen during the TSC measurement.[32] A high bias field drives all the trapped carriers in one direction. Thus a series of measurements of bias TSC gives, in principle, the amount and the centroid of the trapped space charge. The intensity of interfacial $P_4$ TSC peak versus bias electric field from −100kV/cm to +100kV/cm is shown in Fig. 16. The negative polarity of the bias field means that the bias voltage is applied in the direction opposite to the poling field, i.e. EVA(−)-PE(+). For the bias fields from −100kV/cm to +10kV/cm, the intensity of $P_4$ peak remains almost the same. Under the bias fields from +50 to +100kV/cm, $P_4$ peak was not observed. From this experimental result, it is concluded that all the charges at EVA-PE interface responsible for the $P_4$ peak dissipate through the EVA layer under the short circuit condition. This conclusion is reasonable if the charges at the EVA-PE interface are located on the EVA side. This will be proved in Chapter 6.

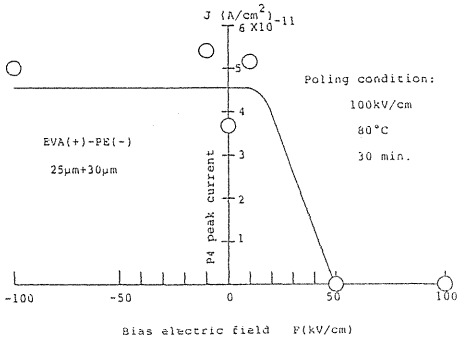


Fig. 16. Dependence of the interfacial peak on bias field.

The integrated charge amount of $P_4$ peak for the poling field of 100kV/cm is $1.8\times10^{-9}$C/cm$^2$ and the resultant internal electric field by the interfacial charges is calculated at about 10kV/cm. This agrees well with the result that the interfacial $P_4$ peak is not observed above +10kV/cm. The fact that the field due to the interfacial charges is about 10% of the applied field implies that the interfacial charges do not distort the internal electric field of EVA-PE composite system so much.

*2. 7. TSC from PE-EVA-PE and EVA-PE-EVA Three Layer Films*

For further information, TSC from a three-layer specimen was investigated. PE and EVA films were put together at room temperature to form specimens with two-layer or three-layer structures. In this report, these specimens are called "two-layer film" and "three-layer film" in contrast to the laminated films whose TSC results are shown in Fig. 6. Figure 17 shows TSC spectra of EVA-PE two-layer films. They are almost the same as those of the EVA-PE laminates in Fig. 6, suggesting that both kinds of specimen have virtually identical interfacial con-

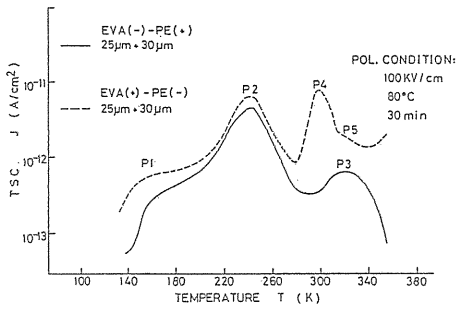


Fig. 17. TSC spectra from EVA-PE two-layer specimens.

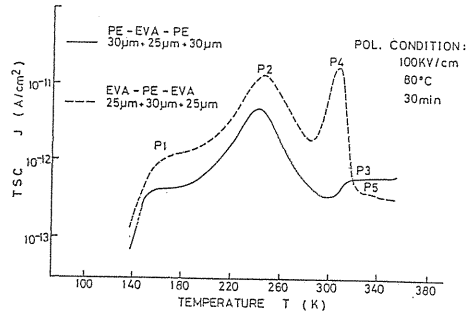


Fig. 18. TSC spectra from EVA-PE-EVA and PE-EVA-PE three-layer specimens.

ditions. This confirms that these two-layer and three-layer films can be used to discuss the nature of the EVA-PE interface.

The TSC spectra of PE-EVA-PE and EVA-PE-EVA are shown in Fig. 18. $P_2$ peak from EVA-PE-EVA is larger than that from PE-EVA-PE. This results from the fact that EVA-PE-EVA contains more vinyl acetate units than PE-EVA-PE and thus contains more dipoles. $P_4$ peak arising from the interface appears only in EVA-PE-EVA, indicating only the interfaces in EVA-PE-EVA act identically with the interface in EVA(+)-PE(−).

### *2. 8. Model of EVA-PE Laminate Films*

The TSC spectra of EVA-PE specimens with Au electrodes show the interfacial $P_4$ peak only in EVA(+)-PE(−). From this result the following two cases are possible, i.e.

(a) positive carriers from the EVA layer are responsible for $P_4$ peak,

(b) negative carriers from the PE layer are responsible for $P_4$ peak.

Further information is obtained from the TSC spectra of tha three-layer films. In Fig. 19 the three-layer films are schematically shown. There are four dielectric-dielectric interfaces, i.e. Ⅰ, Ⅱ, Ⅲ and Ⅳ. Taking the polarity of the poling field into consideration, interfaces Ⅰ and Ⅳ are identical with the interface in EVA(+)-PE(−) for positive carriers in the EVA region. A similar situation exists for interfaces Ⅰ and Ⅳ for negative carriers in

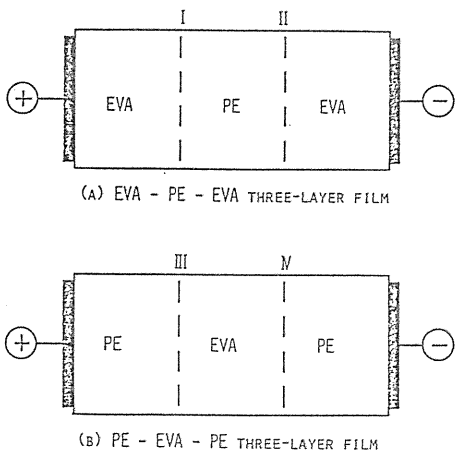


Fig. 19. Schematic diagram of three-layer films.

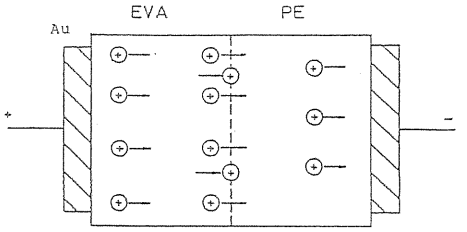


Fig. 20. Model of EVA-PE laminate specimen.

PE. However, the TSC results show that only EVA-PE-EVA shows $P_4$ peak. Therefore, only interface I is identical with the interface of EVA(+)-PE(−). The appearance of $P_4$ peak from interface I but not from interface IV suggests that the carriers responsible for $P_4$ peak are positive carriers injected from the Au anode into EVA (or generated at the anode-EVA interface).

Figure 20 shows a model for a conduction in EVA(+)-PE(−). Positive carriers are injected from the Au anode into EVA and pass through the bulk of EVA. When they reach the EVA-PE interface, part of them are trapped and give rise to $P_4$ peak in the TSC measurement. These phenomena will be discussed further on the basis of conduction current experiments on EVA-PE in Chapter 3.

### *2. 9. Dependence of TSC Spectra on Electrode Metal*

In order to further discuss the origin of the interfacial TSC peak, the dependence of TSC spectra on electrode metal was investigated. The TSC spectra of EVA-PE with Au electrode on the EVA side and Al electrode on the PE side (Au-EVA-PE-Al) are shown in Fig. 21. With this electrode metal arrangement EVA(+)-PE(−) shows the interfacial $P_4$ peak. The appearance of the interfacial TSC peak is not influenced by the electrode metal on the PE side.

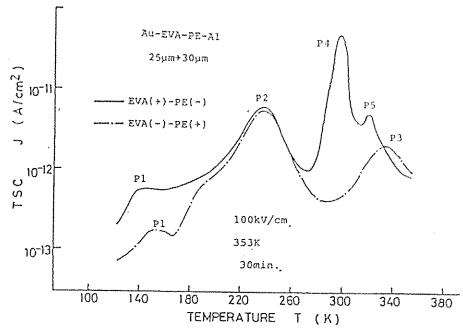


Fig. 21. TSC spectra from Au-EVA-PE-Al.

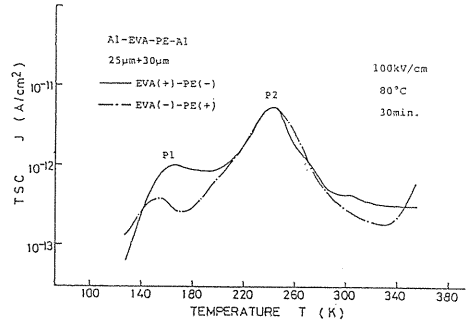


Fig. 22. TSC spectra from Al-EVA-PE-Al.

Figure 22 shows TSC spectra of EVA-PE with Al electrode on both side of the specimen Al-EVA-PE-Al. As shown in this figure, when the Au electrode on the EVA side is replaced by the Al electrode, the interfacial TSC peak disappears, even though a positive voltage is applied on the EVA side (EVA(+)-PE(−)). Therefore, we can conclude that positive carriers injected from Au anode into EVA (or generated at the Au-EVA interface) are responsible for $P_4$ peak. This supports the conclusion obtained in Section 2. 8.

### *2. 10. Dependence of TSC Spectra on Poling Temperature*

Figure 23 shows the dependence of the interfacial TSC peak on the poling temperature.

The $P_4$ TSC peak appears not only when the poling temperature is higher than the $P_4$ peak temperature (290K), but also when the poling temperature is below the peak temperature but above the glass transition temperature (243K). When the poling temperature is above the glass transition temperature ($T_g$), the intensity of

TSC $P_4$ peak is independent of the poling temperature, while $P_4$ peak does not appear when the poling temperature is lower than the glass transition point. This indicates that the positive carriers responsible for $P_4$ peak are mobile only above $T_g$. This result also coincides well with the temperature dependence of the conduction current of EVA (see Section 3. 3.).

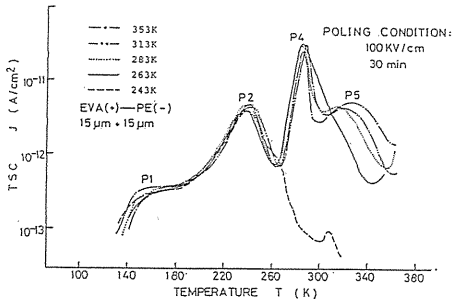


Fig. 23. Dependence of TSC spectra from EVA(+)-PE(−) on poling temperature.

## 3. Electrical Conduction of EVA, PE and Their Composites

### *3. 1. Introduction*

The conduction properties of insulating materials directly influence the quality of electrical insulation. The investigation of conduction properties of polymers is not easy because of complex structures, additives and impurities. If an insulation system is a composite of several dielectric materials, the existence of dielectric-dielectric interfaces is considered to influence the conduction significantly. Furthermore, many polymers are the mixtures of both crystalline and amorphous parts and thus can be considered as composites. Therefore, the study of the effect of dielectric-dielectric interface on electrical conduction is very important.

In this chapter, firstly the conduction properties of single layers of PE and EVA are discussed and then the conduction properties of EVA-PE composites are discussed. The role of semi-conducting layer and the influences of polar groups at the metal-dielectric interface are also discussed in this chapter.

### *3. 2. Experimental*

In order to study the relation between the interfacial TSC peak and conduction currents of EVA, PE and EVA-PE, the condition for the conduction current measurement was chosen to be the same as the poling condition of the TSC experiment (i.e. 343K, 30 minutes).

The procedure for the specimen preparation was the same as in the TSC experiments. The conduction currents were measured with VRE (Vibrating Reed Electrometer, Takeda Riken TR-84M).

### *3. 3. Electrical Conduction of PE*

Since PE is one of the most extensively used insulating polymers, many researchers have studied the electrical conduction of PE[33,34] utilizing dark current, photo-conduction[35], induced conduction by high energy radiation[36], corona charging[37], etc. However, the conduction mechanism of PE in a composite system is not fully understood yet. In order to study the conduction current of EVA-PE composite that of PE, especially its dependence on electrode metal was investigated first.

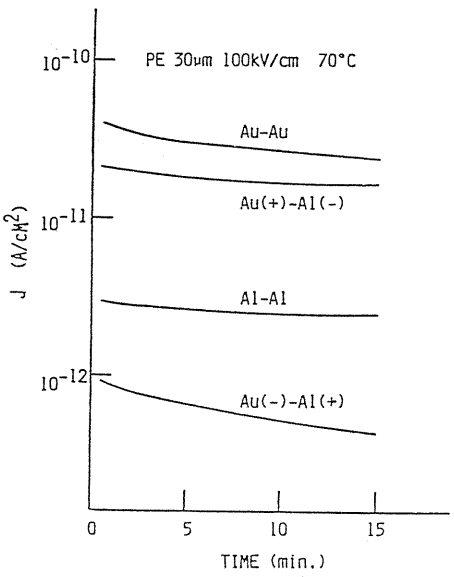


Fig. 24. Dependence of conduction current in PE on electrode metal.

biased Au electrode and negatively biased Al electrode. PE with a positive bias on Au electrode shows relatively high conduction current. The influence of work function of the electrode metal on conduction current suggests that the dominant carriers are mainly supplied by the injection from the metal electrode. The fact that larger conduction current flows when Au electrode is positively biased suggests that holes are injected from Au electrode.

The electric field dependence of conduction current with different electrode metals different polarities are shown in Fig. 25. Although the absolute intensities are different from each other, all of the curves show the same superlinear increase with field.

### 3. 4. *Electrical Conduction of EVA*

The conduction currents of EVA with vinyl-acetate contents from 5.5 wt.% to 22.0 wt.% with gold electrodes were investigated by Yoda[15]. He mainly discussed the temperature dependence of conductivity at low fields (3 kV/cm). In this work, the

Figure 24 shows the electrode metal dependence of the conduction current in PE. The electrode metal dependence of the conduction current in PE is similar to that in EVA. Four curves in Fig. 24 can be divided into two groups:

(1) Au-Au and Au(+)-Al(−) show relatively high conduction currents;

(2) Al-Al and Au(−)-Al(+) show relatively low conduction currents.

Here, for example, Au-Au means the measurement on a specimen with Au electrodes on both sides and Au(+)-Al(−) means that on a specimen with a positively

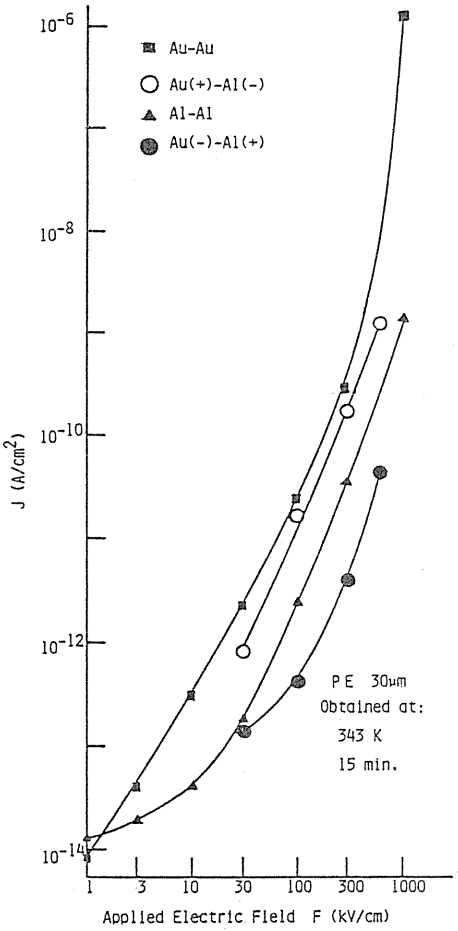


Fig. 25. Dependence of conduction current in PE on electric field and electrode metal.

conduction currents at higher fields were investigated in order to discuss their relation to the interfacial TSC peak which was prominent at poling fields around 100 kV/cm.

The dependence of the conduction current on electrode metal is shown in Fig. 26. The four curves in Fig. 26 are divided into two groups.

In the cases of Au-Au and Au(+)-Al(−) (i.e. with positive voltage on Au electrode) EVA shows a high conduction current, while in the cases of Al-Al and Au(−)-Al(+) EVA shows a low conduction current. The difference in conduction current reaches two orders of magnitude. The conduction currents in PE (cf. Section 3.3.) and the conduction currents in EVA with Al-Al or Au(−)-Al(+) have the same order of magnitude. The metal-EVA interface, thus strongly influences the conduction properties of EVA.

In order to exclude the possibility for an impurity to play a role in conduction, the conduction current of EVA after hexane treatment was also measured. The hexane treatment to remove impurities was carried out by immersing EVA films in hexane at 333 K for 2 hours. The resultant conduction currents were almost the same as those from EVA without hexane treatment. This revealed that larger conduction currents of EVA with Au anode result from the properties of EVA itself, but not from the impurities involved.

The conduction current of Au(+)-Al(−) is almost the same as that of Au-Au. The less influence of the cathode metal on conduction current implies that in the cases of Au(+)-Al(−) and Au-Au the dominant carriers are positive carriers from the anode. As the work functions of Au and Al are 5.1~5.5 eV and 4.0~4.4 eV, respectively[38], it is reasonable that Au electrode acts as a good hole-injecting electrode.

Figure 27 shows electric field dependence of Au-Au Au(+)-Al(−), Al-Al,

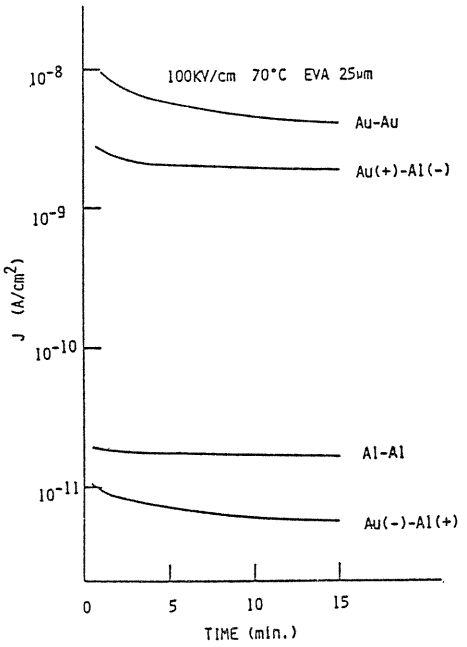


Fig. 26. Dependence of conduction current in EVA on electrode metal.

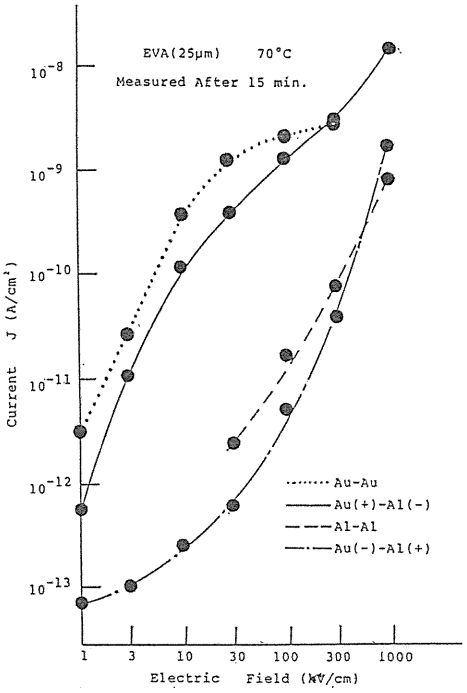


Fig. 27. Dependence of conduction current in EVA on electric field and electrode metal.

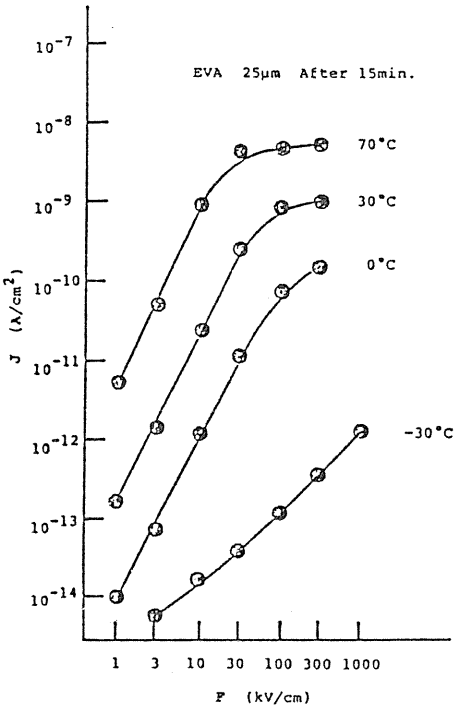


Fig. 28. Temperature dependence of conduction currents in EVA.

and Au(−)-Al(+). The two groups mentioned in Section 3. 3 also show different field dependences. The conduction currents from Au-Au and Au(+)-Al(−) tend to saturate at electric fields above ca. 30 kV/cm. However, those from Al-Al and Au(−)-Al(+) do not show the tendency to saturate but keep increasing superlinearly with field as is usually seen in various insulating materials, e.g. PE (cf. Section 3. 3.). These indicate that the high current and the saturation tendency of EVA are the nature of the conduction or the injection of the positive dominant carriers.

The field dependences of conduction current at different temperatures are shown in Fig. 28. The saturation tendency occurs above the glass transition temperature of EVA. Below the glass transition temperature, the current increases superlinearly with field. This suggests that the conduction or the injection of the positive carriers are dominant above the glass transition temperature.

### *3. 5. Electrical Conduction of Laminae Films*

In Chapter 2, TSC spectra of EVA-PE laminate films were discussed and they showed strong polarity dependence. The model of EVA-PE laminate film was also proposed from the polarity dependence and the electrode metal dependence. In this section the properties of EVA-PE will be discussed from the view point of conduction current, and the model of EVA-PE suggested in Chapter 2 will be reconfirmed.

In Fig. 29 the conduction currents of EVA(+)-PE(−) and EVA(−)-PE(+) laminate films are compared with those of EVA and PE. All of the specimens in this figure have Au electrodes. The conduction current of EVA is larger than that of PE by two orders of magnitude. When positive voltage is applied on the EVA side of the laminate (EVA(+)-PE(−)), the conduction current in EVA-PE has the same order of magnitude as that of EVA. In EVA(−)-PE(+) the conduction current has the same order of magnitude as that of PE.

The field dependence of the conduction current EVA-PE is shown in Fig. 30. The conduction in EVA(+)-PE(−) shows the same tendency to saturate around 100 kV/cm as EVA. That in EVA(−)-PE(+) does not tends to saturate but increases super-lineally like PE. The similarities of the magnitude and the field dependence of conduction current between EVA and EVA(+)-PE(−) suggests that in the case of EVA(+)-PE(−) the properties of EVA determine the conduction in EVA-PE.

The conduction currents of EVA-PE with different electrode metal arrange-

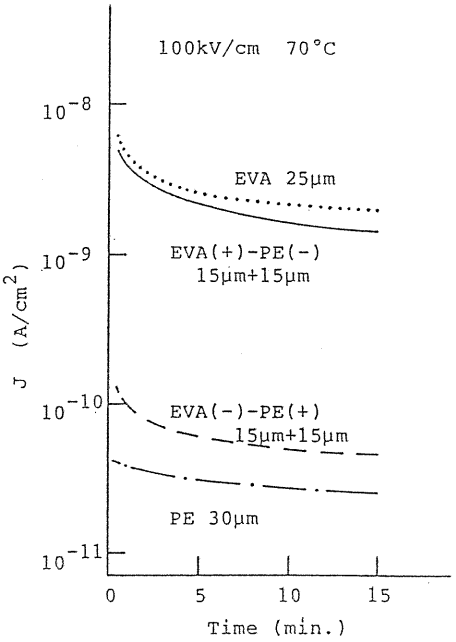


Fig. 29. Conduction currents of EVA, PE and EVA-PE laminate films.

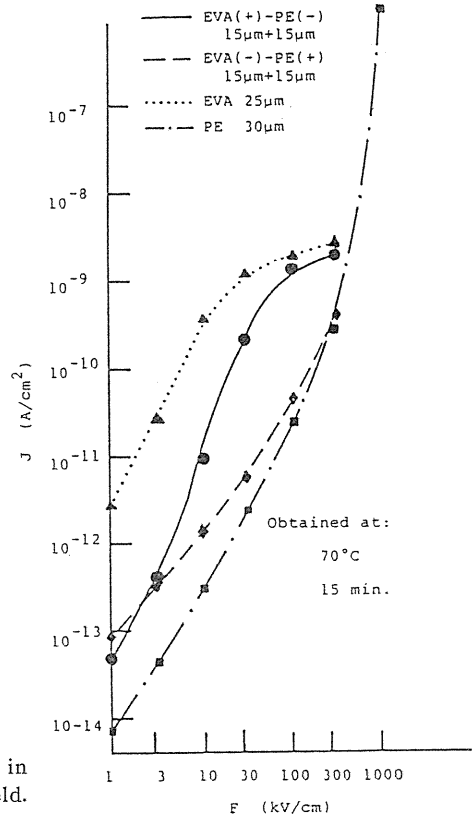


Fig. 30. Dependence of conduction currents in EVA, PE and EVA-PE on electric field.

ments are shown in Fig. 31. EVA(+)-PE(−) with Au-Au electrodes and Au(+)-EVA-PE-Al(−) show larger conduction currents and EVA-PE with Al-Al electrodes and Al(+)-EVA-PE-Au(−) show smaller conduction currents. The difference in conduction current between the above two groups also reaches two orders of magnitude. From this result we can conclude that larger conduction current in EVA-PE requires a positively biased Au anode on the EVA side.

This also implies that electrode metal on the PE side has less influence on the conduction current of EVA-PE and the EVA-PE interface does not influence the motion of positive carriers much. The fact that positive biasing of the EVA layer with a Au electrode results in a larger conduction current in EVA-PE clearly shows that positive carriers injected from

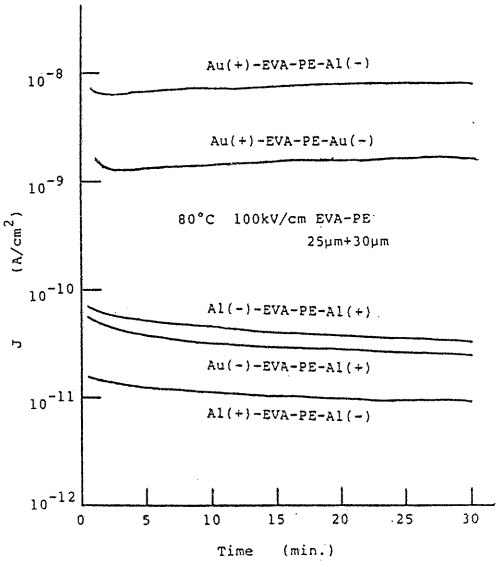


Fig. 31. Dependence of conduction currents in EVA-PE on electrode metal.

the Au anode are the dominant carriers in EVA-PE. These conclusions are consistent with those obtained in Chapter 2 from TSC measurements. These results also show that in the case of EVA(+)-PE(−) the positive carriers injected from the Au anode into EVA easily pass through the EVA-PE interface, though some of them are trapped at the interface, giving rise to an interfacial TSC peak. After entering the PE bulk, these carriers easily move inside the PE bulk, resulting in a larger conduction current in EVA-PE. The apparent conductivity of the PE layer is increased by about two orders of magnitude by the neighbouring EVA layer which acts as an "electrode" injecting positive carriers into PE layer. It is interesting that dielectric layer (EVA) inserted between PE and Au electrode does not increase the resistance of the insulating system but on the contrary it decreases the resistance by assisting carrier injection. Thus, the interface plays a very important role in the conduction of the composite.

The conductivity of an insulating material has conventionally been measured by using a slab of the material with metal electrodes on both sides. However, as in a composite system each component layer does not have metal electrodes on both sides but is in contact with other dielectrics, the conductivity of each layer in a composite may differ from that measured in a conventional way.

In Chapter 2 the relation between TSC spectra of PE-EVA-PE, EVA-PE-EVA three layer films and those of EVA-PE two layer films was discussed. The conduction currents of two and three layer films were also measured in order to compare them with those of one and two layer films. Figure 32 shows the conduction currents in PE-EVA-PE and EVA-PE-EVA three layer films together with those in EVA-PE, EVA and PE. Regarding the magnitude of the conduction current in Fig. 32, the currents are divided into the following two groups. EVA, EVA(+)-PE(−) and EVA-PE-EVA show large conduction currents, and PE, EVA(−)-PE(+) and PE-EVA-PE show small conduction currents. In Chapter 2, the TSC of EVA-PE-EVA and PE-EVA-PE three layer films and EVA-PE two layer films were divided into two groups, i.e. EVA-PE-EVA and EVA(+)-PE(−) showing the TSC peak originating from the EVA-PE interface and PE-EVA-PE and EVA(−)-PE(+) not showing the TSC peak originating from the EVA-PE interface. The resemblance of these two classification of multi-layer films suggests the close relation between TSC and conduction current. The multi-layer film having the small conduction current does not show the interfacial TSC peak. This may be because in these systems the density of the carrier is not high enough to cause an interfacial charge accumulation responsible for the TSC peak.

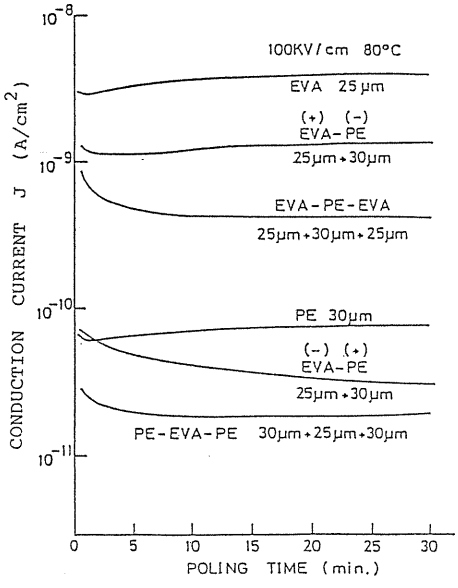


Fig. 32. Comparison of conduction currents in EVA-PE-EVA, PE-EVA-PE with those in EVA, PE and EVA-PE.

### *3. 6. Model of Conduction of EVA-PE Laminate Films*

In Section 2. 8. a model was proposed to explain the polarity dependence and the electrode metal dependence of the TSC spectra in EVA-PE films. The same model is also possible to explain the results of the conduction currents.

The large conduction currents in the EVA(+)-PE(−) and EVA-PE-EVA and the small conduction currents in EVA(−)-PE(+) and PE-EVA-PE are explained by the models in Figs. 33 and 34. The large conduction currents in Au(+)-EVA-PE-Au(−) and Au(+)-EVA-PE-Al(−) are caused by the positive carriers (holes) injected from the Au anode into EVA. These positive carriers easily pass through the EVA-PE interface and enter the PE bulk. After entering the PE bulk these positive carriers move in the PE bulk easily and increase the conduction current in the PE bulk by about two orders of magnitude. In EVA-PE-EVA these positive carriers again pass through the PE-EVA interface and enter the EVA bulk on the cathode side.

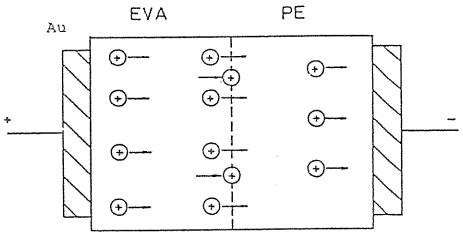


Fig. 33. Model for conduction in EVA-PE laminate film.

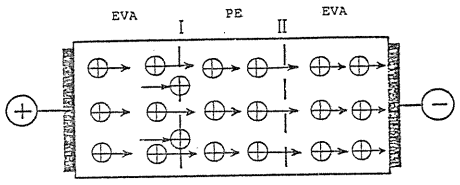


(A) EVA - PE - EVA THREE-LAYER FILM

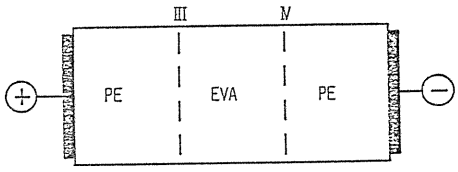


(B) PE - EVA - PE THREE-LAYER FILM

Fig. 34. Model for conduction in EVA-PE-EVA and PE-EVA-PE.

As Au has a larger work function than Al, it is reasonable for holes to be injected from the Au anode into EVA easily. The small conduction currents in Au(−)-EVA-PE-Au(+) and Al(+)-EVA-PE-Al(−) are ascribed to less hole injection from Au into PE and from Al into EVA. The small conduction current in PE-EVA-PE is ascribed to small hole injection from Au anode into the PE layer.

### *3. 7. Conduction Current of EVA with Semi-Conducting Layer*

As mentioned in the previous sections positive-carrier injection plays an important role in the conduction of EVA, PE and their composite films. In certain cases a dielectric layer may act as a carrier-injecting electrode (e.g. EVA(+)-PE(−)). Thus, the properties of the metal-dielectric and dielectric-dielectric interfaces are very important in the electrical insulation system.

The polymeric semi-conducting layers, which are made by mixing conducting particles with polymers, are widely used in practical UHV XLPE (cross-linked PE) cables in order to avoid the breakdown caused by defects (voids, protrusions, etc.) at the conductor-dielectric interfaces. In this section the conduction current of EVA with semi-conducting layer was investigated in order to clarify the role of semi-conducting layer in electrical conduction.

The polymeric semi-conducting layer used in the experiment was made by mix-

ing 50 wt.% of acethylene black with EVA. The semi-conducting layer was formed by hot press and its thickness was ca. 400 $\mu m$. Its conductivity is ca. $10^{-3}$ S/cm. Since the semi-conducting layer has much higher conductivity than EVA, the voltage across the EVA layer is considered to be the total applied voltage to the EVA-semi-conducting layer composite.

Figure 35 shows the conduction currents in the two-layer specimens composed of EVA and semi-conducting layer (in the figure "SC" represents "semi-conducting layer") with different electrode materials. For the ease of comparison, the results obtained from single EVA layer without semi-conducting layer are also shown in this figure. As shown in Fig. 35, when a positive voltage is on EVA (SC(−)-EVA (+)), the conduction currents show electrode metal dependence similar to that of EVA and have almost the same magnitude as those in EVA. This implies that in the case of SC(−)-EVA(+) the conduction current is determined by positive carrier injection from anode metal into EVA and that there is less influence of the semi-conducting layer. When a negative voltage is on EVA (SC(+)-EVA(−)), the conduction current does not depend on the electrode metal. The magnitude of the conduction current is smaller than that of EVA with Au electrode but larger than EVA with Al electrode. This implies that in the case of SC(+)-EVA(−), positive carrier injection takes place from semi-conducting layer into EVA and the rate of injection is between those from Au and Al. This coincides with the fact that the work function of carbon is 5.0 eV lying between the work functions of Au (5.1～5.5 eV) and Al (4.0～4.4eV)[38]. Furthermore, the interfaces of SC-Al and SC-Au have less influence on the conduction current of the SC-EVA composites. This suggests that the interface between metal and semi-conducting layer has less influence on the conduction current.

For further information conduction currents of EVA with graphite (Aquadag) electrode were measured and the results are shown in Fig. 36. The results have a tendency similar to Fig. 35. This indicates that positive carriers are injected from

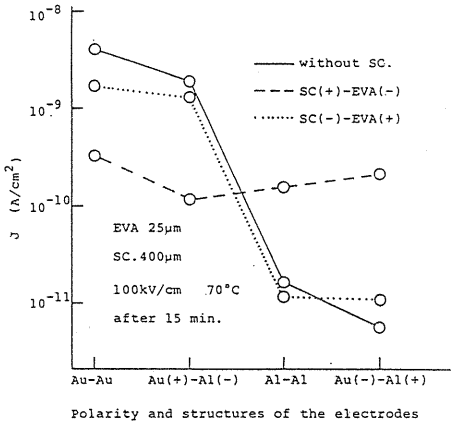


Fig. 35. Conduction currents in EVA with semi-conducting layer and EVA.

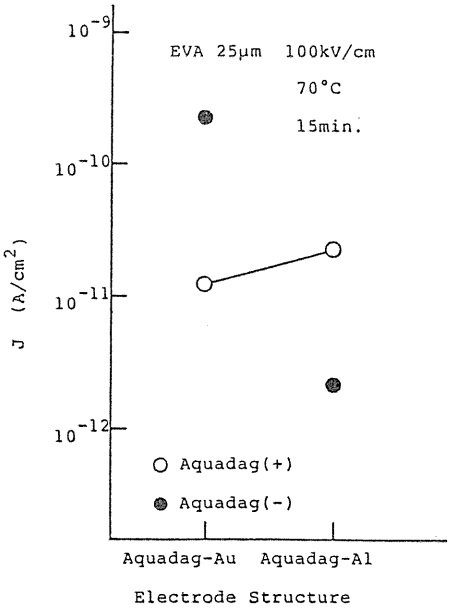


Fig. 36. Dependence of conduction currents in EVA on electrode metal.

the graphite electrode into EVA and that the rate of injection lies between those from Au and Al electrodes. The absolute values of the currents in Fig. 36, however, are smaller than those in Fig. 35. This seems to arise from poor wettability of the EVA surface to water, as Aquadag (colloidal graphite) was used by dissolving graphite powder in water. Therefore, the effective area of contact of graphite electrode with EVA is considered to be less than the nominal electrode area.

The above experimental results revealed that influence of a polymeric semi-conducting layer on conduction is determined by the work function of conductive particles mixed in the polymeric matrix of the semi-conducting layer.

### *3. 8. Effects of Polar Groups on Electrical Conduction in Polyethylene*

The experimental results obtained from the conduction current and TSC measurements revealed that positive carriers are easily injected into EVA from Au anode. EVA is basically polyethylene containing polar vinyl acetate units. Figure 37 shows the dependence of the conduction current in EVA film on the vinyl acetate (VAC) content. Conduction current increases with vinyl acetate content. This implies that the introduction of acetoxy groups into PE enhances the positive carrier injection. This suggests the importance of polar groups on the carrier injection process. In this section the carrier injection via polar groups into PE[39] will be discussed.

In order to study the role of polar group, PE film with a cast layer of EVA, oxidized PE or polyvinyl alcohol (PVA) were used as a specimen. Oxidized PE is obtained by exposing PE films to an ozone atmosphere at room temperature. The solvent used to cast EVA and oxidized PE was tetrahydrofuran (THF) while that

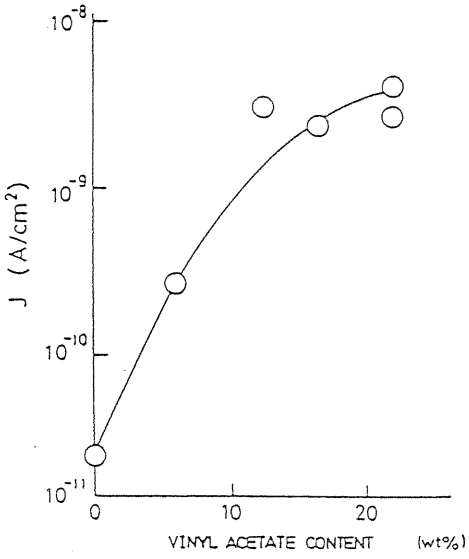


Fig. 37. Dependence of conduction currents in EVA on vinyl acetate content (100kV/cm, 343K, 15minutes after voltage application).

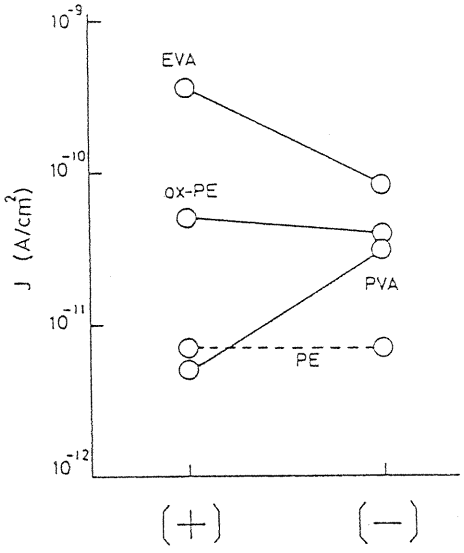


Fig. 38. Conduction currents in PE with surface layer containing polar groups (100 kV/cm, 343K, 15minutes after voltage application). The + and − in parentheses show the polarity of applied voltage on the surface-layer side of specimen.

for PVA was pure water. The thickness of the cast layer was estimated to be about 1 $\mu m$. The electrodes were evaporated gold. The effect of THF on conduction currents seems negligible, since no change in conductivity was observed in a PE film which had undergone wetting with THF prior to the vacuum evaporation of the electrodes.

The results of conduction current measurements are shown in Fig. 38. The PE specimen with a surface layer containing acetoxy groups shows larger conduction current than that without the surface layer by about two orders of magnitude when a positive voltage is applied to the surface layer (SL(+)). This suggests that the acetoxy groups enhance positive carrier injection. The conduction current with a negative voltage on the surface layer (SL(−)), however, is also larger than that in PE by about an order of magnitude. This suggests that the introduction of acetoxy groups incidentally enhance negative carrier injection, though positive carrier injection is dominant.

In PE with an oxidized PE surface layer, the conduction currents were equally increased for both SL(+) and SL(−). This suggests that oxidation products, possibly carbonyl groups, enhance both positive and negative carrier injection.

The introduction of the PVA surface layer increases the conduction current only in SL(−), which implies the hydroxyl groups enhance negative carrier injection.

Polar groups have been reported to influence the contact electrification of polymers. Acetoxy groups and hydroxyl groups enhance the positive charging of PE,[40,41] whereas oxidation products enhances negative charging.[42] The relation between these reports and the results given here is not clear, and further work is needed on this point.

Yumoto et al. reported the effect of polar groups on the carrier injection into PE[43] by observing the surface potential decay of the corona-charged specimen. In contrast with our results, they concluded that the existence of polar groups generally suppresses the carrier injection. This difference may arise from the difference in the injection mechanism, since in corona charging, the carrier injection has been reported to be assisted by factors other than the electric field, such as corona light or active molecules[44,45].

The existence of some polar groups at the metal-PE interface region is considered to enhance carrier injection into PE: acetoxy groups mainly enhance positive carrier injection; oxidation products such as carbonyl groups enhance both positive and negative carrier injection; and hydroxyl groups enhance negative carrier injection. Possible mechanisms of the enhancement of carrier injection are (i) the introduction of localized states due to polar groups via which carriers are injected[46] and (ii) modification of the energies of localized levels by the existence of polar groups[47].

## 4. Discharge Currents in EVA Film and EVA-PE Laminate Films

### *4. 1. Introduction*

In Chapters 2 and 3 the polarity dependences of TSC spectra and conduction current of EVA-PE were discussed. From those discussions it was shown that in EVA-PE the simple Maxwell-Wagner model[1] can not be used to calculate the internal electric field and the charge accumulation at the EVA-PE interface.

Therefore, it is necessary to investigate the space charge accumulation in EVA-PE experimentally. The charge accumulation in dielectric is possible to be investigated by the TSC measurement. The investigation of TSC after DC field application proved successful[2,3,48,26]. The TSC results in EVA-PE composite (see Chapter 2) also provided information on space charge accumulation in the composite. For further information and in order to clarify the space charge accumulation under AC and DC field application, isothermal discharge currents after DC and AC field application were investigated.

From an engineering point of view, the investigation of the charge accumulation under AC voltage application is important, since most of insulating composites are used under AC voltage application.

### *4. 2. DC Discharge Currents of EVA-PE*

The discharge current in EVA-PE after a DC voltage application was measured at various temperatures for various applied voltages and polarities.

The amount of discharged charge was approximated by the integration of discharge current over the interval from 0.5 minute to 15 minutes after short-circuiting.

#### *4. 2. 1. Released Charges Calculated from $P_4$ TSC Peak and Discharge Current*

As $P_4$ TSC peak is relatively sharp, we assume that $P_4$ peak is a single-relaxation-time process. The relaxation time $\tau$ is expressed by

$$\tau(T)=\tau_0\exp(H/kT) \qquad (15)$$

and at peak temperature $T_m$

$$\tau(T_m)=\tau_0\exp(H/kT_m)=kT_m^2/\beta H. \qquad (16)$$

where $\tau_0$ is a constant, H the activation energy, k Boltzmann's constant, $\beta$ the temperature rising rate (6 K/min).[49]

The activation energy of $P_4$ was calculated at 1.5 eV from the initial rise method. According to equation (16), at peak temperature $T_m$ (290 K for $P_4$), the relaxation time is 48 seconds. The temperature at which current was measured was chosen to be 273 K. At 273 K the relaxation time for the $P_4$ peak is 33 minutes. On the other hand, as shown in Fig. 39, the discharge current continues to decrease over more than 15 minutes. Both the $P_4$ peak and the discharge current at 273 K have similar relaxation times and they are considered to be dominated by the same depolarization mechanism. The

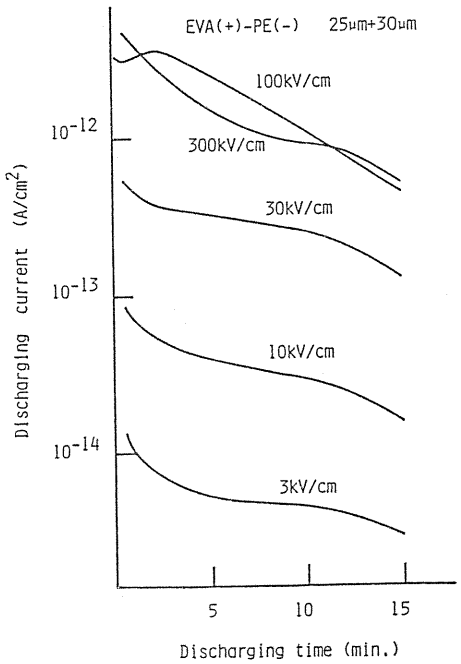


Fig. 39. Dependence of discharge currents in EVA(+)-PE(−) at 273K on electric field.

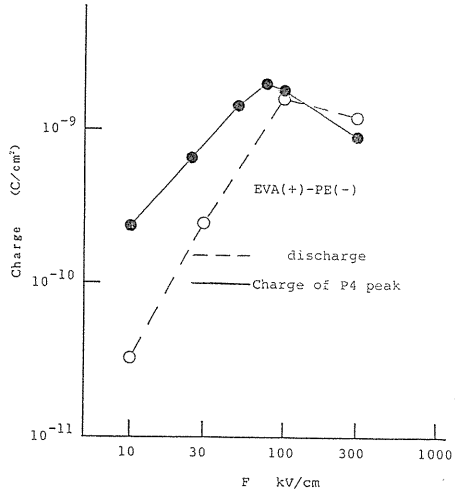


Fig. 40. Electric field dependence of released charges calculated from the discharge currents at 273K and from TSC $P_4$ peak.

released charge calculated from the discharge current (from 0.5 to 15 minutes) is considered to be a little less than the total released charge. But, for simplicity, in this chapter, the charges integrated over the interval from 0.5 to 15 minutes are used to discuss the relation between TSC and discharge current.

Figure 39 shows discharge currents of EVA(+)-PE(−) at 273 K. The discharge current increases with applied field and decreases at fields higher than 100kV/cm. This is similar to the field dependence of the intensity of $P_4$ TSC peak. The total charges calculated from the TSC and the discharge current are plotted in Fig. 40. The two curves coincide well both qualitatively and quantitatively.

### *4. 2. 2. Released Charges Calculated from $P_5$ TSC Peak and Discharge Current*

In order to find out the relation between discharge current and $P_5$ TSC peak, the discharge current of EVA(+)-PE(−) at 343K were measured. To determine the temperature suitable for the measurement of discharge current responsible for

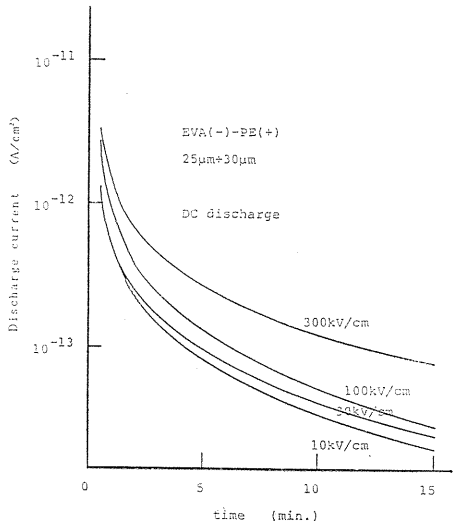


Fig. 41. Dependence of discharge currents in EVA(−)-PE(+) at 343K on electric field.

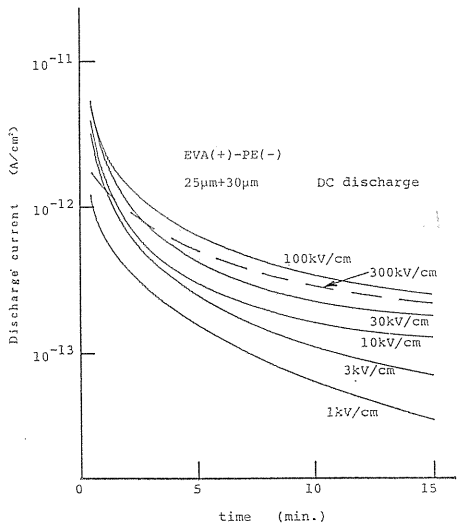


Fig. 42. Dependence of discharge currents in EVA(+)-PE(−) at 343K on Electric field.

the $P_5$ peak is rather difficult because the influence of the $P_4$ peak just below the $P_5$ peak can not be completely avoided. If the discharge current is measured at temperatures lower than the $P_5$ peak temperature, the discharge responsible for the $P_4$ peak should be taken into account. The time constant for $P_4$ peak at 343K is calculated at 0.004 s. Therefore, the integration of discharge current at 343 K from 0.5 minute to 15 minutes is considered not to be affected by the discharge corresponding to the $P_4$ TSC peak. The discharge current measured at 343K, thus, reflects the accumulated charge which is released around and above the $P_5$ peak temperature.

The discharge currents of EVA-PE at 343 K are shown in Figs. 41 and 42. The discharge currents of EVA(−)-PE(+) in Fig. 41 are smaller than those of EVA(+)-PE(−) in Fig. 42. The big difference in intensity implies that EVA(−)-PE(+) accumulate less charges than EVA(+)-PE(−). This result also coincides well with the TSC results.

The electric field dependence of discharge current of EVA-PE shows strong polarity dependence. The discharge current of EVA(−)-PE(+) in Fig. 41 monotonously increases with applied field, while the discharge current of EVA(+)-PE(−) in Fig. 42 increases with field below 100 kV/cm and decreases above 100 kV/cm. This tendency is similar to the field dependence of the released charge at 273 K. However, as the relaxation time of the $P_4$ TSC peak is 0.004s at 343K, as mentioned above, the charge released at 343 K does not relate to the $P_4$ TSC peak.

Figure 43 shows the electric field dependences of charges calculated from $P_5$ TSC peak and the discharge currents at 343 K. Both of them have similar tendencies. Therefore, it is reasonable to conclude that the dependence of the released charge on electric field at 343 K results from the charge accumulation which is responsible for $P_5$ TSC peak.

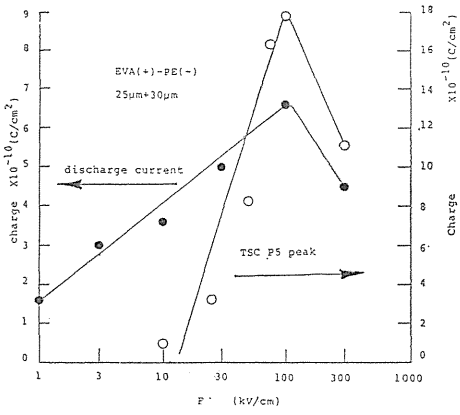


Fig. 43. Electric field dependence of released charges calculated from the discharge currents at 343 K and those from $P_5$ TSC peak.

*4. 3. AC Discharge Current of EVA-PE and EVA*

TSC and discharge current measurements were carried out on specimens poled with AC voltages. The procedure of TSC experiment was as follows. At a poling temperature an AC voltage applied to the specimen was increased with a voltage increasing rate of 10 % of the final applied voltage per second and was kept at the final voltage for 30 minutes (poling process). Then, the specimen was cooled to the liquid nitrogen temperature and the voltage was decreased at the same rate as that of the voltage increase. The procedure for the following TSC measurement was the same as that after DC voltage application.

TSC method was powerful for the study of charge accumulation in EVA-PE poled with a DC voltage. However, TSC after AC voltage application showed no TSC peaks. The reason is considered as follows. The polarity of AC field changes

50 or 60 times per second under commercial power frequency. The rapid polarity change may lead to a small amount of a space charge. Furthermore, as the polarity dependence of the conduction in EVA-PE is large at high temperature but is small at low temperature, it is likely that during the cooling process of the TSC experiment the polarity change may cancel the space charge polarization already accumulated in the composite. These seem the reasons why the measured TSC curve after AC voltage application showed no TSC peak. However this does not mean that a space charge is not accumulate at all by AC voltage application at the poling temperature. Therefore, the isothermal measurement of discharge current after AC voltage application was carried out in an attempt to obtain information on the space charge under AC voltage.

In the discharge current measurement, AC voltage (60 Hz) was carefully applied by increasing and decreasing the voltage at a rate of 10 % of the final applied voltage per second, in order to avoid the effect of phase angle of voltage application and removal. The applied AC voltage was kept constant for 15 minutes.

Figure 44 shows the charge obtained by integrating the discharge current after AC voltage application over the interval from 0.5 to 15 minutes. In the same figure the released charge from EVA-PE after DC voltage application and the released charge of EVA after AC application are also plotted. The AC electric field was characterized by its peak voltage. The direction of discharge current in EVA-PE was always from EVA to PE in the external circuit. The amounts of released charges were strongly dependent on the applied field as shown in Fig. 44. The accumulated charge increases as the applied AC field increases. The released charge from the two-layer specimen coincides well with that from the laminate specimen. This implies that the difference of interfacial condition between two-layer and laminate specimens has less influence on the charge accumulation under AC voltage application. This suggests that the accumulation takes place not in the EVA-PE interfacial region but in EVA or PE bulk or metal-polymer interfaces. The temperature dependence of the accumulated charge under AC field is shown in Fig. 45.

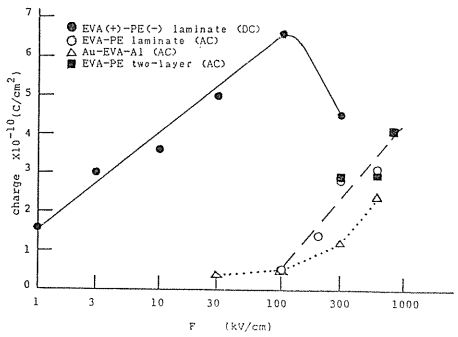


Fig. 44. Electric field dependence of released charge from EVA-PE laminate after AC voltage application at 343K.

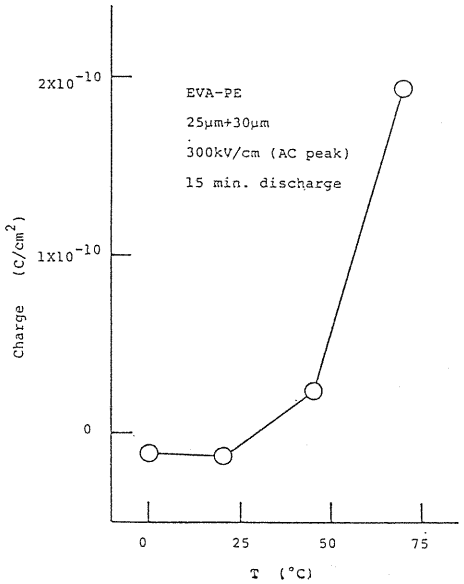


Fig. 45. Temperature dependence of released charges from EVA-PE two-layer film after AC voltage application.

The charge amount is very small at low temperatures. This is considered to result from the fact that the conduction in EVA-PE under a DC voltage does not depend much on polarity at low temperatures.

The TSC and conduction current of EVA-PE under DC voltage have remarkable polarity dependence at 343K (cf. Chapters 2 and 3). Therefore, the charge accumulation is considered to take place under AC voltage application at 343 K as follows. The positive-carrier injection takes place in the cycle of EVA(+)-PE(−) and the positive carriers tend to move back in the cycle of EVA(−)-PE(+). Some of the injected positive carriers are trapped in the bulk of EVA. The remaining trapped carriers give rise to the discharge current after AC field application.

The discharge currents in Au-EVA-Au and those in Au-EVA-Al are shown in Figs. 46 and 47. The discharge current of EVA with Au-Au electrodes seems to result from temperature gradient, because turning the same specimen upside-down has no influence on the direction of the discharge current. This current has less transient part than the discharge current from Au-EVA-Al and quickly reaches a small steady current. The large transient current in EVA with Au-Al electrodes is considered to result from the asymmetric electrode arrangement. In Au-EVA-Al, as mentioned in Chapter 3, positive carriers can be injected from the Au electrode in the period of Au(+)-EVA-Al(−) and the injected carriers may not be completely discharged in the period of Au(−)-EVA-Al(+), which results in larger discharge current after short-circuiting. On the other hand, in Au-EVA-Au, positive carriers can be injected from the both sides and the remaining positive charges are located symmertrically in the specimen. This leads to a very small discharge current and the temperature gradient inside the specimen may contribute to the current.

The field dependence of released charges in Au-EVA-Al after AC voltage application is shown in Fig. 44, which is similar to that in EVA-PE after AC voltage application. This suggests that the processes of charge accumulation both systems are the same. Since the polarity of the field changes rapidly under AC field

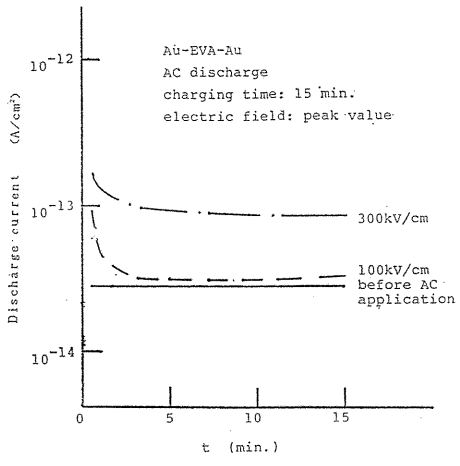


Fig. 46. Discharge current of EVA (with Au-Au electrodes) after AC voltage application.

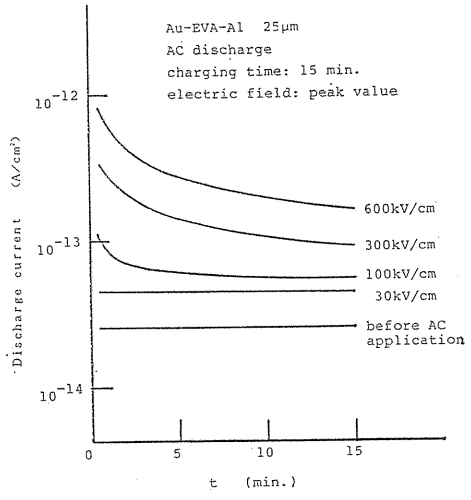


Fig. 47. Discharge current of EVA (with Au-Al electrodes) after AC voltage application.

application, the injected charges have not enough time to penetrate far from the electrode. Therefore, in EVA-PE and Au-EVA-Al under AC voltage application, positive-carrier accumulation is considered to take place in the bulk of EVA and/or in the Au-EVA interface region. This explains the facts that (i) the EVA-PE laminate and the two-layer film give the same released charge and (ii) the field dependence of the released charge after AC voltage application is completely different from that after DC voltage application where charges are accumulated at the EVA-PE interface.

## 5. Breakdown Strength of EVA-PE Laminate Films

### *5. 1. Introduction*

In the previous chapters it was described that the EVA-PE composite showed strong polarity dependences of conduction current and TSC around 100 kV/cm at temperatures around 343 K. However, as shown in Fig. 27, the conduction current tends to be less dependent on the polarity of the applied voltage as electric field exceeds 100 kV/cm. The interfacial $P_4$ TSC peak also shows the similar tendency and decreases as the poling field exceeds 100 kV/cm. For the practical application of composite insulating systems, it is important to understand the influence of the polarity on the breakdown strength and the internal electric field of EVA-PE. Although the internal electric field in a composite which shows a polarity dependence can not be calculated from the Maxwell-Wagner model, it can be evaluated by certain methods[50~52]. In this chapter, the internal field in EVA-PE under very high field has been estimated from breakdown experiments.

### *5. 2. DC Breakdown Strength*

The electrodes of the specimens used in breakdown experiments were evaporated gold. The electrodes were with diffused edges and 5 mm in diameter on one side and 20 mm in diameter on the other side.

DC breakdown strength ($F_b$) was measured by applying a ramp voltage of 500 V/s and $F_b$ was evaluated by averaging results of no less than 20 measurements.

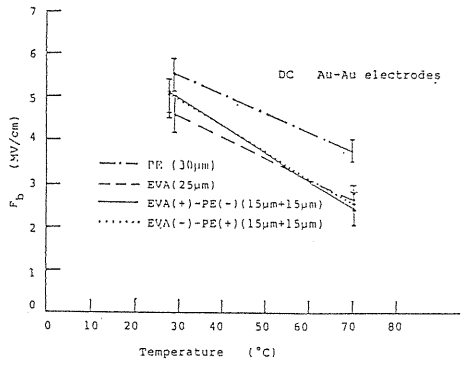


Fig. 48. Temperature dependence of DC breakdown strength of PE, EVA and EVA-PE (voltage rising rate: 500 V/s).

Figure 48 shows the DC breakdown strengths ($F_b$) of EVA-PE laminate, PE and EVA films at room temperature and 343 K. At room temperature $F_b$'s of EVA-PE laminates lie between those of PE and EVA and at 343 K they are close to those of EVA. Unlike the TSC and the conduction current, $F_b$ of EVA-PE laminate shows no polarity dependence. This seems reasonable since the conduction current of EVA-PE shows less polarity dependence at higher fields around 2 MV/cm. This seems to arise from less difference in conduction current between PE and EVA at higher fields.

For simplicity, we neglect the field distortion due to space charge in each layer and the thickness dependence of dielectric strength. We also assume that the whole laminate breaks down when an internal field of one of the composing layers reaches its own dielectric strength. These allow to estimate the internal fields at the breakbown. The relations between internal fields are summarized in Table 2 for the following likely cases. Here $F_{PE}$ and $F_{EVA}$ are the internal fields in the PE and EVA layers, respectively and $F_{bPE}$ and $F_{bEVA}$ are the breakdown strengths of the PE and EVA layers, respectively.

Table 2. Relation between internal fields and breakdown strength.

| | relation between $F_{PE}$ and $F_{EVA}$ | region of initiation of breakdown | $F_b$ |
|---|---|---|---|
| (1) | $F_{PE}=F_{EVA}$ | EVA | $F_{bEVA}$ |
| (2) | $F_{PE}\gg F_{EVA}$ | PE | $\frac{F_{bPE}}{2}$ |
| (3) | $F_{PE}>F_{EVA}$ | EVA and PE | $\frac{F_{bEVA}+F_{bPE}}{2}$ |

The case (1) in Table 2 is a case where the internal field of PE is the same as EVA. As the breakdown strength of EVA is lower than PE at both room temperature and 343 K, the breakdown strength of the composite is determined by the breakdown strength of EVA. This case is possible if the conductivity of the PE layer is increased by the existence of neighbouring EVA layer as in the case of EVA(+)-PE(−) around 100 kV/cm.

The case (2) is based on the idea that the internal field of a laminate specimen is determined by the conductivities of each layer. This is based on the Maxwell-Wagner model.

The case (3) corresponds to the "optimum voltage division" in the laminate specimen. The word "optimum voltage division" is used here to describe the case in which the internal fields of both layers in the laminate reach their own breakdown strength at the same time. This is desirable voltage division for a composite insulating system. In this case, a laminate shows the highest breakdown strength among the three cases.

Other cases such as a case where the internal field in EVA is higher than PE seems less possible, because the conductivity of a single EVA layer is higher than PE.

Figure 49 shows the experimental data and the calculated breakdown strengths of EVA-PE laminates for the three cases mentioned above. At room temperature

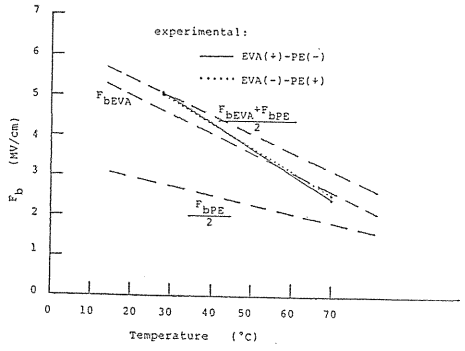


Fig. 49. Calculated breakdown strengths for the three cases in Table 2 and the experimental results.

the breakdown strength is close to that for the "optimum voltage division" case. This suggests that the optimum voltage division is the case at room temperature. However, at 343 K the breakdown strength differs from that for the optimum voltage division and is close to $F_{bEVA}$. This implies that the breakdown mechanism at high temperature region may be different from that at room temperature.

The internal fields of EVA and PE can be calculated directly from the experimental breakdown strength for the following two cases.

case (i): the internal field in the EVA layer first reaches its breakdown strength.

case (ii): the internal field in the PE layer first reaches its breakdown strength.

The ratios of internal fields of PE to EVA ($F_{PE}/F_{EVA}$) at room temperature for both cases (i) and (ii) are ca. 1.2, as shown in Fig. 50. This implies that the internal fields in both PE and EVA layers reach their own breakdown strengths almost at the same time. Since $F_{bPE}/F_{bEVA}$ is about 1.2 at room temperature. At 343 K this ratio is about 1 for case (i) and 3.1 for case (ii).

In order to determine the internal field ratio at 343K, the field dependences of the conduction currents in EVA and PE were measured under a ramp voltage with the voltage rising rate of 30 V/s. Figure 51 shows the results. At high fields near breakdown strength, although the difference between the conduction currents of EVA and PE becomes small, the conduction current of PE seems to remain smaller than that of EVA. Therefore, the ratio $F_{PE}/F_{EVA}$ of 3.1 seems more reasonable, although this value can not directly obtained from Fig. 51. Therefore, the breakdown of the PE layer seems to determine the breakdown strength of the PE-EVA laminate at 343 K.

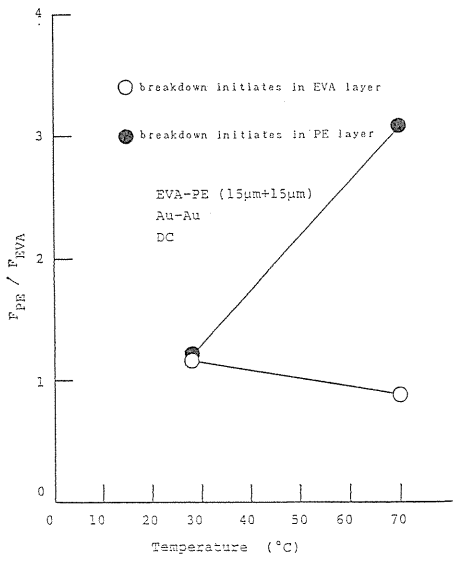


Fig. 50. Calculated ratio of internal fields $F_{PE}/F_{EVA}$.

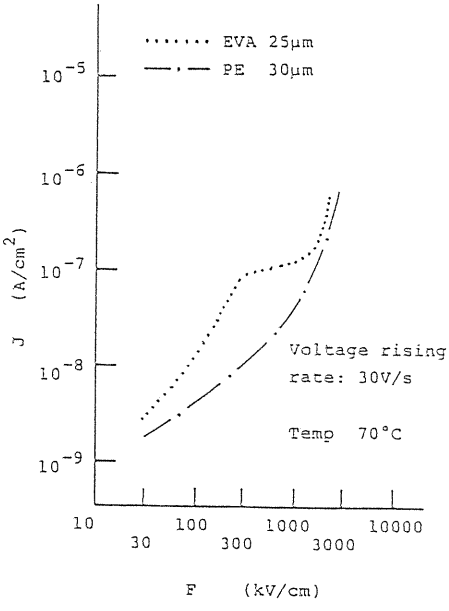


Fig. 51. Conduction currents of EVA and PE under a ramp voltage with a voltage rising rate of 30V/s.

*5. 3. Impulse Breakdown Strength*

The impulse breakbown strength of the EVA-PE laminate film was also measured in order to clarify the internal electric field of each layer under the application of an impulse voltage.

The intensity of the impulse voltage was so selected that the breakdown takes place within 5 $\mu s$, i. e. the breakdown takes place in the wave front.

The impulse breakdown strength of the EVA-PE laminate is shown in Fig. 52. The impulse breakdown strengths of the EVA and PE single layer films are also plotted together. Like the DC breakdown strength the impulse breakdown strength has no polarity dependence either at room temperature or at 343 K.

At room temperature, the impulse breakdown strengths of PE and EVA are ca. 5 MV/cm and 4 MV/cm, respectively and the breakdown strength of EVA-PE laminate film is ca. 4. 5 MV/cm for both polarities. The ratio of internal fields in PE and EVA ($F_{PE}/F_{EVA}$) is 1. 25 at room temperature. The breakdown strength of 4. 5 MV/cm for EVA-PE is obtained only in the case of "optimum voltage division".

At 343 K, the impulse breakdown strengths of EVA, PE and EVA-PE are almost the same (ca. 4 MV/cm). This implies that the ratio of internal field in EVA to PE in the EVA-PE laminate is about 1. This also is the case of optimum voltage division. Therefore, it is concluded that under the impulse voltage application the ratios of internal field in EVA-PE laminates are optimum at both room tem-

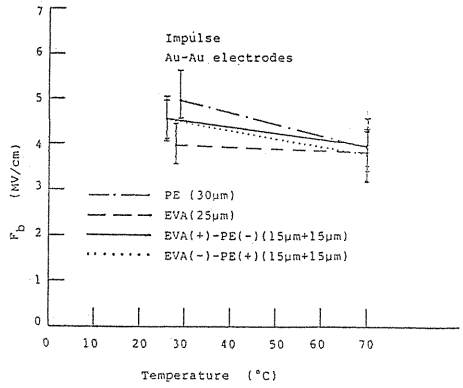


Fig. 52. Breakdown strength of EVA-PE under impulse voltage application.

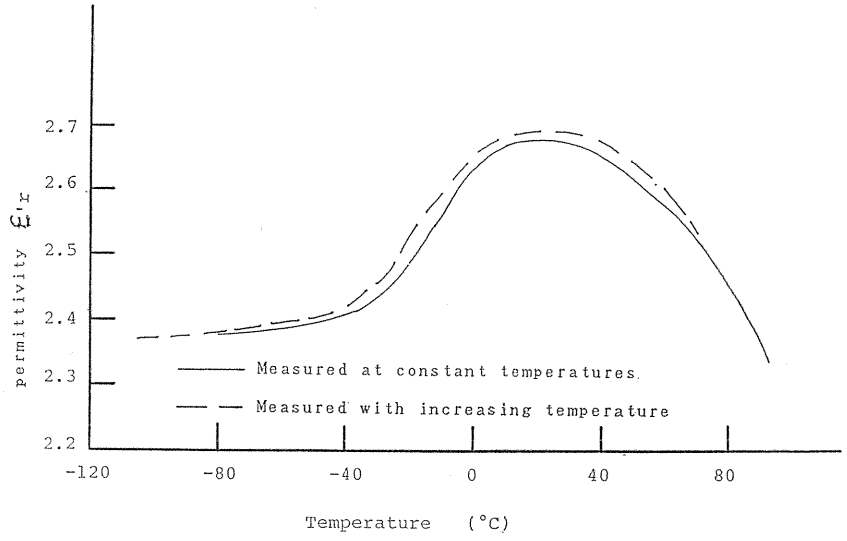


Fig. 53. Temperature dependence of relative permittivity of EVA.

perature and 343 K.

Assuming that the voltage division in EVA-PE is determined by the capacitance of each layer, the permittivity of EVA can be calculated by using the relative permittivity of PE (2.3). The calculated relative permittivity of EVA was 2.8 at room temperature and 2.3 at 343 K. The measured relative permittivity of EVA at 1 kHz is shown in Fig. 53. The equivalent frequency for the impulse voltage is estimated at about 40 kHz. The calculated relative permittivity of EVA shows good agreement with the measured relative permittivity. Therefore, it is concluded that under an impulse voltage the voltage division of the EVA-PE laminate film is determined by capacitance of each layer.

DC breakdown strengths of single layers of EVA and PE, however, are different from impulse breakdown strengths. This may be due to the influence of space charge. The above simple models are based on the assumption that effects of space charge and thickness can be neglected. Therefore, it should be noted that the above calculation is rough estimation.

## 6. Evaluation of Internal Electric Field by Separation Method

### *6. 1. Introduction*

There are a few methods to evaluate the internal electric field utilizing electron beam, Kerr effect, pressure pulse, thermal pulse[50~53] and so forth. In Chapter 5 a method to evaluate the internal field from breakdown strength was proposed. It is useful for the evaluation of the internal electric field at high fields near breakdown strength. In order to clarify the internal electric field under an applied field lower than the breakdown field, the "separation method" can be used. The separation method is to evaluate the internal field by measuring an intensity of a dipolar TSC peak from a single component layer of a multi-layer composite. The principle and the details of this method will be given in the next section.

### *6. 2. Separation Method*

TSC spectrum of an electret containing dipoles shows dipolar peaks whose intensity increase linearly with the poling electric field as described in Chapter 2. Therefore, if a laminate insulating film has at least one layer containing dipoles, it is in principle possible to evaluate the internal electric field by the following procedure.

(a) Two films are put together in vacuum at room temperature to form a two-layer composite (lamination process).

(b) The laminate film is poled at a certain temperature.

(c) The laminate film is cooled to a temperature at least lower than the peak temperature of the dipolar TSC peak under consideration.

(d) The laminate film is separated at this low temperature and a metal electrode is brought into contact with a surface of the separated layer in order to make a TSC measurement.

(e) By comparing the intensity of the dipole peak of the separated film with the linear dependence of the peak on the poling field obtained for a single-layer specimen, the internal field can be evaluated.

An equipment for this measurement was developed. Figure 54 is the front

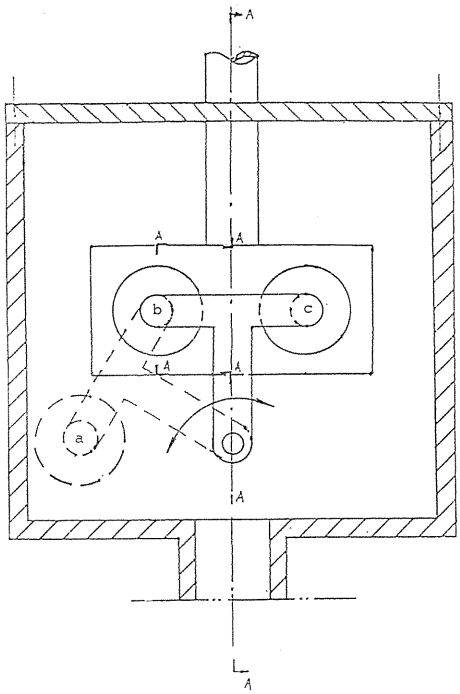


Fig. 54. Front cross sectional view of equipment for the separation method.

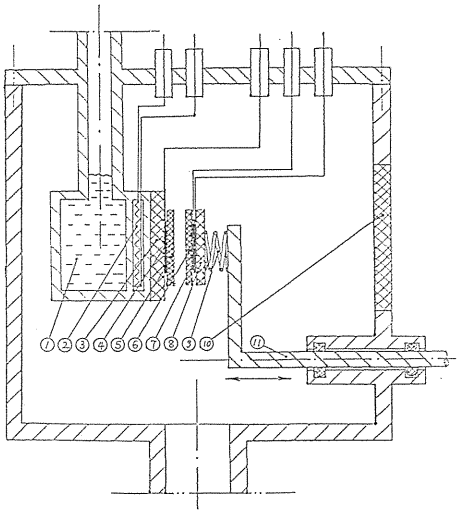


Fig. 55. Cross-section at A-A in Fig. 54.

cross sectional view of the equipment and Fig. 55 shows the cross section at A-A in Fig. 54. The crank shaft inside a vacuum vessel can be moved toward right or left as shown in Fig. 55 and can be turned as shown in Fig. 54. Component films of a composite ((5) and (6) in Fig. 55) are placed on two electrodes ((4) and (7)), one of which is fixed to a spring on the crank shaft. By moving the crank shaft the film (6) is pressed on the film (7) to form a two-layer composite (lamination). During the separation an operator pulls the crank shaft outward without turning it to separate the two-layer film. After removing the layer at position "b", the crank shaft was turned counter-clockwise (cf. Fig. 54). The separated part then moved from position "b" to "a". An electrode or a dielectric layer with an electrode moves from position "c" to "b" to make a contact with the remaining layer at "b". Of course, the electrode or the layer at position "c" is cooled to the same temperature as the specimen at "b" before hand. All of the operations including lamination and separation are performed in vacuum. The movable electrode is supported by a spring (9) which ensures the contact between the specimen and the electrode or between the upper dielectric layer and the lower one. During the lamination or the separation an operator is able to observe the specimen through the observation window (10). Other structures of this equipment for measuring TSC are similar to an ordinary one.

### *6. 3. Accuracy of Separation Method*

The accuracy of the internal field evaluation by the separation method is

affected by many factors such as contact electrification, interfacial polarization, mechanical deformation and cooling rate.

In separating at two-layer insulating system the contact electrification[54~59] may cause a problem. However, the charge penetration depth in contact electrification was estimated to be shallow (ca. 300nm)[54]. This penetration depth is about 1/100 of the specimen thickness. Therefore, after contacting an electrode and short-circuiting the specimen, the charge due to the contact electrification has a negligible influence on the internal field of the bulk and, thus, on the intensity of the dipolar peak even if the charge due to contact electrification moves back to electrode during the TSC measurement. The influence of electrification caused by the separation was investigated by measuring TSC spectrum from a PE or EVA film separated without poling. No TSC peak was observed and this indicates that there was no influence of contact electrification on the TSC spectrum.

In the separation method, the interfacial charges accumulated during the poling seem to have no influence on the TSC spectrum for the same reason as above.

The absolute intensity of $P_2$ peak in the separated EVA layer from EVA-EVA is smaller than that from the poled single layer of EVA. This is considered to be due to mechanical deformation. The influence of mechanical deformation is confirmed by the change in capacitance. Figure 56 shows the temperature dependence of capacitance of the separated EVA layer. One side of the separated EVA layer is in contact with a solid electrode, not with an evaporated electrode. In order to know the influence of the change in permittivity with temperature the change in permittivity of EVA is also shown in the same figure. The permittivity of EVA increases at glass transition temperature of EVA and the capacitance also increases reflecting this increase in permittivity. However, at higher temperatures, in spite that the permittivity slowly decreases, the capacitance still increases. This result implies that though the permittivity plays a role in capacitance change, the change in capacitance mainly results from the change in distance between electrodes. The separation at liquid nitrogen temperature results in mechanical deformation of the separated specimen and this makes an uneven contact between specimen and contact electrode since the specimen is hard at low temperature. Therefore, the resultant distance between electrodes becomes larger than the film thickness. As temperature increases the hardness of specimen decreases and the force due to the spring attached to the upper electrode decreases the distance between electrodes.

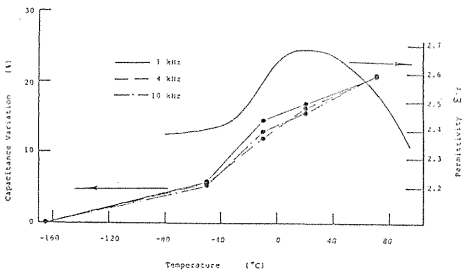


Fig. 56. Temperature dependence of capacitance of separated EVA layer and that of permittivity of EVA.

The change in distance between electrodes causes the change in TSC peak intensity and finally results in an error in the internal field evaluation. The maximum change in electrode distance was estimated at about $-20\%$ from the change in capacitance. The intensities of $P_2$ dipolar peak for a single layer of EVA and the separated EVA layer from the EVA-EVA two-layer film revealed that the total error resulting from the overall separation procedure is a little more than the above estimate and reaches about $-40\%$. Considering the error ($-40\%$) resulting

from the separation method, the data given in the following sections have been calibrated by increasing them by 40 %.

The composite has different field distributions at different temperatures. Therefore, a slow cooling rate, which is not high enough to freeze in the field distribution at the poling temperature, results in errors. The appearance of TSC peak due to carriers near the dipole peak also results in errors in the internal field estimation. Therefore, these problems have to be taken into account carefully when the separation method is applied.

### *6. 4. Internal Field Evaluation from Dipolar TSC Peak*

In order to estimate the internal field distribution accurately it is required that trapped carriers do not affect the dipolar peak and that the peak is large. The $P_2$ peak of EVA seems to meet the requirements. The $P_2$ peak intensities of the separated EVA layers from EVA-EVA two-layer film are the same. which supports the reliability of the separation method.

Figure 57 shows the TSC spectra of the separated EVA, which was polarized in the form of EVA-PE composite and separated from the PE layer at liquid nitrogen temperature. The poling temperature was 253 K in order to measure the internal field around the glass transition point of EVA and PE. The TSC spectra clearly show the dipolar peaks around 243 K. The two curves show no polarity dependence. As the $P_2$ TSC peak of EVA around 243K results from dipoles[26] (cf. Section 2. 4.) and has linear dependence on applied field (cf. Fig.9), it is possible to evaluate the internal field. When an average field of 100 kV/cm was applied to the EVA-PE composite, the resultant internal field of the EVA layer was ca. 70 kV/cm (before calibration: 40 kV/cm). The internal field of the PE layer is then calculated at ca. 130 kV/cm.

The ratio of the internal fields between EVA and PE in both EVA(+)-PE(−) and EVA(−)-PE(+) are around 1 : 2 (before calibration 1 : 4). The TSC spectra in Fig. 57 show no polarity dependence and this also implies the voltage divisions for both polarities are the same. Figure 58 shows the conduction currents in EVA -PE, EVA and PE at 243 K. The conduction currents of EVA-PE show no polarity

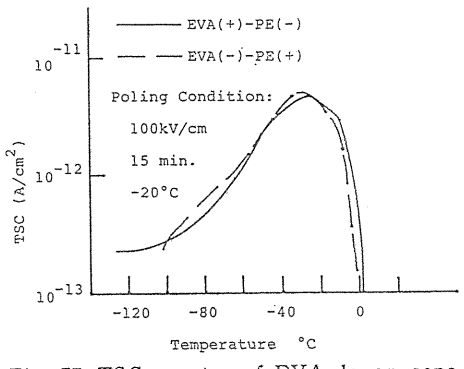


Fig. 57. TSC spectra of EVA layer separated from EVA-PE polarized at 253 K.

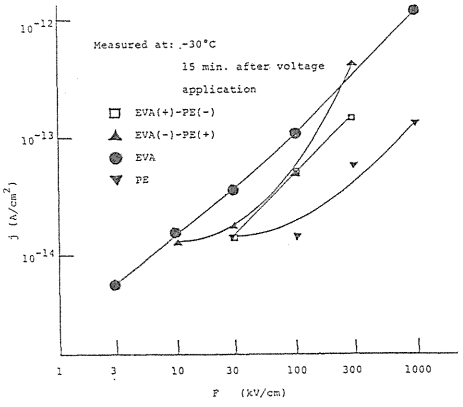


Fig. 58. Electric field dependence of conduction currents of EVA, PE and EVA-PE at 243 K.

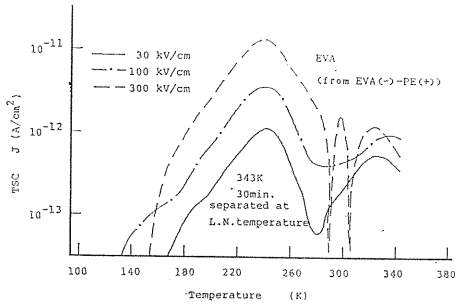


Fig. 59. TSC spectra of EVA separated from EVA(−)-PE(+) polarized at 343 K.

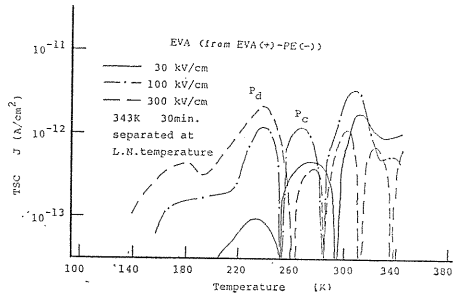


Fig. 60. TSC spectra of EVA separated from EVA(+)-PE(−) polarized at 343 K.

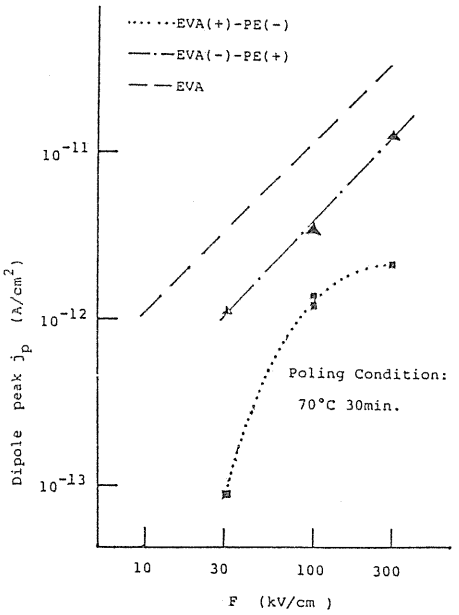


Fig. 61. Field dependence of dipolar TSC peaks of EVA separated from EVA-PE and EVA single layer.

dependence around 243 K under an electric field of about 100 kV/cm. The conduction current of EVA is larger than that of PE. The results of the separation experiments agree well with the results of conduction current measurements around this poling temperature in Fig. 58.

It is reasonable that the internal field in EVA is smaller than that in PE, since (i) the conduction in EVA is larger than that in PE and (ii) the positive carrier injection into EVA, which affects the conduction in the neighboring PE layer is not dominant around 243K.

On the other hand, this dipole peak shows strong polarity dependence, when poling temperature is 343 K as shown in Figs. 59 and 60. This implies that the voltage division depends on polarity at higher temperatures.

Figure 59 shows the TSC spectra of the EVA layer, which were polarized at 343 K in the form of EVA-PE with a negative voltage on the EVA side (EVA (−)-PE(+)) and separated at liquid nitrogen temperature. The dipole peaks around 243 K show linear dependence on the poling field as shown in Fig. 61. Internal electric fields of EVA are 50 % (before calibration 30 %) of the average fields of EVA-PE.

Figure 60 shows the TSC spectra of the EVA layer from EVA-PE poled under the same conditions as for Fig. 59 except that the polarity is opposite (EVA(+)-PE(−)). Unlike the case of EVA(−)-PE(+), TSC spectra show peaks Pc adjacent to dipole peak $P_2$. which are considered to be due to carriers since the direction is opposite to that of normal depolarization current. The appearance of Pc peak strongly influences the apparent intensity of dipole peak $P_2$. Therefore, the accurate evaluation of internal electric field is difficult in this case. However, in spite of

the existence of Pc, qualitative estimation is still possible. Figure 61 shows the electric field dependence of $P_2$ dipole peak of EVA(−)-PE(+) and EVA(+)-PE(−). The dipole peak of EVA(+)-PE(−) is smaller than that of EVA(−)-PE(+). The smaller dipole peak implies a lower field in the EVA layer. Therefore, it is reasonable to conclude that the internal field of EVA are smaller in EVA(+)-PE(−) than in EVA(−)-PE(+) at 343 K. This implies that the internal field distribution is dependent on the polarity of the applied voltage.

### *6. 5. Location of Charges Responsible for Interfacial TSC Peak in EVA(+)-PE(−)*

In Chapter 2, the $P_4$ TSC peak in EVA(+)-PE(−) was shown to result from positive carriers trapped at the EVA-PE interfacial region. However, the exact location of these positive carriers in the interfacial region is not easy to determine from TSC measurements. The separation method can provide further information on the location of the carriers.

The procedure was as follows. After the poling and the cooling of an EVA-PE two-layer specimen the applied field was removed and one of the layers of the two layer-film was removed. Then, a non-polarized layer of the same material was brought into contact with the remaining layer to form a new two-layer system. The TSC measurement was carried out on the new two-layer system.

Figure 62 shows the TSC of EVA-PE (EVA(+)-PE(−)) whose one layer was replaced by a fresh layer. Replacing PE layer gives less influence on the intensity of interfacial TSC peak around 290 K than replacing EVA layer. This suggests that main part of the interfacial positive carriers responsible for the $P_4$ peak are on the EVA side of the interface. The TSC peak around 240 K in solid line is considered to result from the orientation of dipoles in EVA layer under the influence of the PE layer.

The solid line in Fig. 63 shows the TSC spectra of EVA-PE (EVA(−)-PE(+)), whose PE layer was replaced at liquid nitrogen temperature. This does not differ much from the TSC of EVA(−)-PE(+) specimen whose layers were not replaced. This shows that three TSC peaks ($P_1$, $P_2$ and $P_3$) in EVA(−)-PE(+) result from

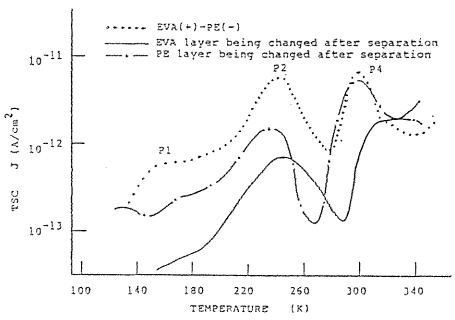


Fig. 62. TSC spectra of EVA-PE, one layer of which was replaced by a fresh film after the poling (EVA(+)-PE(−)) at 343K and the separation at liquid nitrogen temperature.

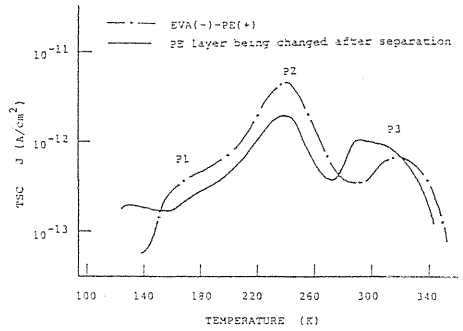


Fig. 63. TSC spectra of EVA-PE whose PE layer was replaced by a fresh film after the poling (EVA(−)-PE(+)) at 343 K and the separation at liquid nitrogen temperature and EVA(−)-PE(+).

EVA layer as shown in Chapter 2.

## 7. TSC and Conduction Current of Other Combinations of Polymers

### *7. 1. Introduction*

In Chapters 2 to 6 the EVA-PE laminate films were studied. The TSC spectra and conduction currents of EVA-PE composite showed strong polarity dependences and, therefore, the simple Maxwell-Wagner model can not be applied to analyze the EVA-PE composite. However, there are some reports which explained the composite insulating system by the Maxwell-Wagner model[2,3]. It is important to clarify whether the polarity dependence of TSC and conduction current in the EVA-PE composite is a rare exception or not. For this reason, TSC spectra and conduction currents from other combinations of polymers were also studied.

### *7. 2. TSC and Conduction Currents of EVA-HDPE, EVA-PP, EVA-FEP and EVA-PET*

HDPE (high density polyethylene), PP (polypropylene), FEP (fluorinated ethylene-propylene copolymer) and PET (polyethylene terephthalate) were used in the measurements. The physical properties of these materials are summarized in Table 1. The conduction current measurement and the poling for TSC are carried out under the electric field of 100 kV/cm at 353 K.

Figures 64 and 65 show the TSC spectra of EVA-HDPE and EVA-PP, respectively. The TSC spectra of HDPE and PP single-layer films are too small to appear in these figures. The TSC spectra depend on the polarity of the applied field and the interfacial $P_4$ peak is observed around 290 K only when the specimens are poled with a positive voltage on the EVA side. Figures 66 and 67 show the conduction currents of EVA-HDPE and EVA-PP laminate films, respectively. The conduction currents show remarkable polarity dependence similar to that of EVA-PE. The conduction current is much larger with a positive voltage on the EVA side than with a negative voltage on the EVA side. Therefore, the model of conduction for EVA-PE in Chapter 3 is also applicable to the cases of EVA-HDPE and EVA-PP.

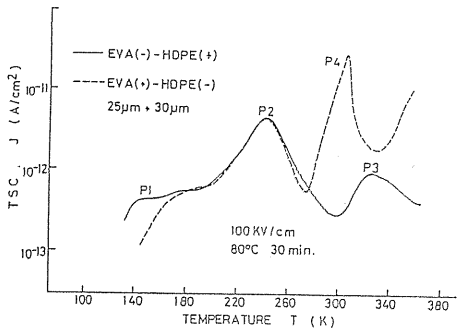


Fig. 64. TSC spectra from EVA-HDPE two-layer films.

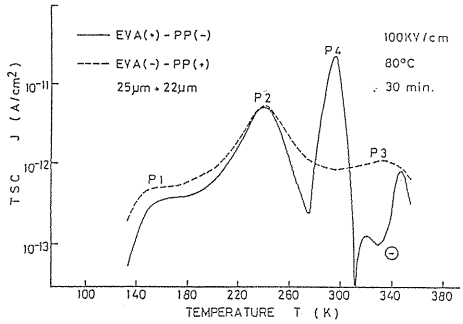


Fig. 65. TSC spectra from EVA-PP two-layer films.

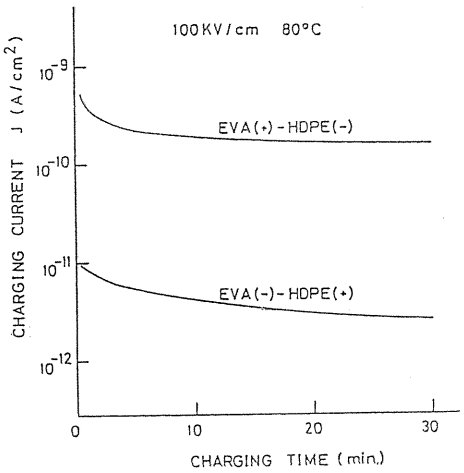


Fig. 66. Conduction currents in EVA-HDPE two-layer films.

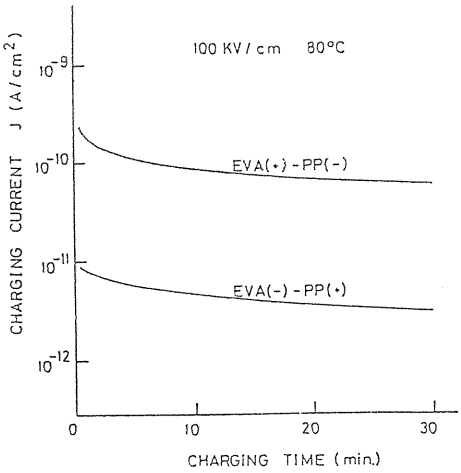


Fig. 67. Conduction currents in EVA-PP two-layer films.

Figures 68 and 69 show TSC spectra and conduction currents of EVA-FEP, respectively. These show another type of the polarity dependence. When a positive voltage was applied on the EVA side, TSC spectrum of EVA-FEP does not show a new interfacial peak but the intensity of a TSC peak around 290 K in EVA(+)-FEP(−) is larger than that in EVA(−)-FEP(+). The conduction current in EVA(+)-FEP(−) about 20 minutes after voltage application is smaller than that of EVA(−)-FEP(+). However, at initial stage the conduction current in EVA(+)-PE(−) is larger than that of EVA(−)-PE(+).

Figures 70 and 71 show TSC spectra and conduction currents in EVA-PET They do not show the polarity dependence. The model for EVA-PE can not be applied to the case of EVA-PET under 100 kV/cm at 353 K.

In conclusion the model proposed for the TSC and conduction in EVA-PE com-

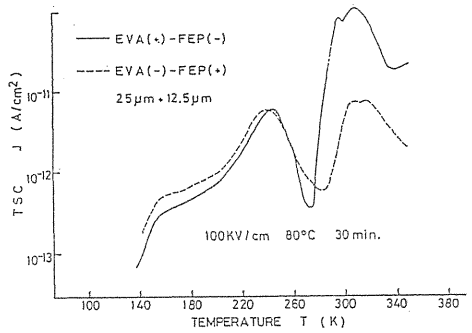


Fig. 68. TSC spectra from EVA-FEP two-layer films.

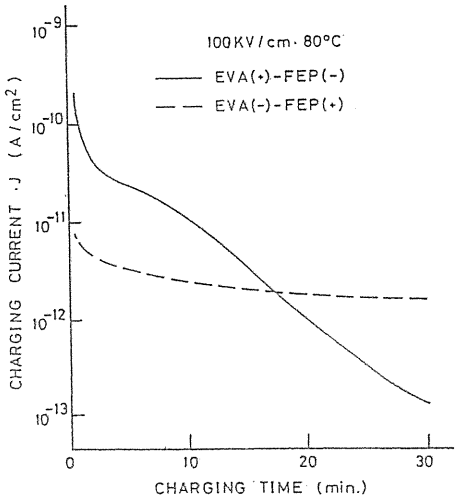


Fig. 69. Conduction currents in EVA-FEP two-layer films.

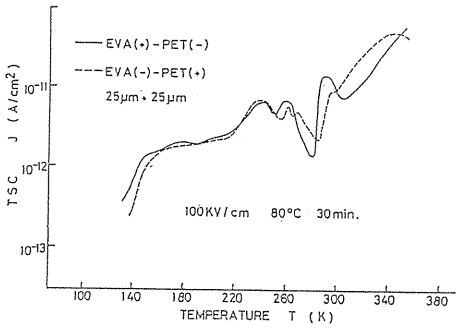


Fig. 70. TSC spectra from EVA-PET two-layer films.

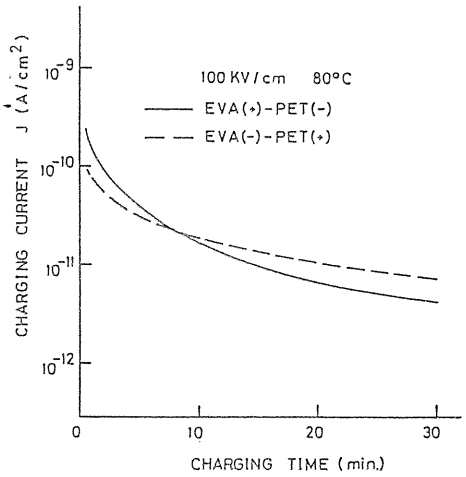


Fig. 71. Conduction currents in EVA-PET two-layer films.

posite is also applicable to some other polymer-polymer composites. This suggests that the influence of the interface is very important in the polymer composite system.

## 8. Conclusion

In order to clarify the effects of interface in a polymer-polymer composite insulating system, TSC, conduction current and dielectric breakdown measurements were carried out on EVA-PE and other composite films. The main conclusions obtained in this research are summarized as follows.

TSC and conduction current in EVA-PE showed remarkable dependence on the polarity of the applied field and electrode material. This is explained by the following model. Positive carriers are easily injected into EVA from the Au anode. Some of them are trapped at the EVA-PE interface and give rise to the interfacial TSC peak. Most of the positive carriers can pass through the EVA-PE interface and move in the PE layer, increasing the conduction current in PE by about two orders of magnitude. In such systems as EVA-PE, the simple application of the conventional Maxwell-Wagner model leads to wrong conclusions. The existence of some polar groups at the metal-PE interface is considered to enhance carrier injection into PE.

The measurements of discharge currents after DC or AC voltage application were carried out. The difference in discharge current between DC and AC poling suggests different mechanisms and locations of the trapped carriers for DC and AC poling.

The internal fields in EVA-PE composite under high fields near dielectric breakdown were estimated by measuring dielectric strength. Under DC voltage the ratios of internal fields of PE and EVA are 1.2 at room temperature and 3.1 at 343 K. Under impulse voltage the voltage division is determined by the permittivity of each layer.

The internal fields in EVA-PE under the fields below the breakdown strength were estimated by the separation method, which was developed here. The ratio of internal fields of PE and EVA is about 2 at 243 K for both EVA(+)-PE(−) and EVA(−)-PE(+). At 343 K it is about 3 for EVA(−)-PE(+) and higher for EVA (+)-PE(−). This method also revealed that the positive carriers trapped at the EVA-PE interface region were located on the EVA side.

The strong polarity dependence of TSC and conduction current was also observed in other combinations of polymer materials. This indicates that EVA-PE is not an exceptional case to show the strong polarity dependence and that the application of the Maxwell-Wagner model should be carefully done to analyze practical composite insulating systems.

## Acknowledgements

The authors would like to express their gratitude to Mitsubishi Petrochemical Co. Ltd. for the supply of EVA, LDPE, HDPE and EVA-PE laminate films. This work was supported in part by a Grant-in-Aid for Scientific Research from the Ministry of Education, Science and Culture. The authors are also grateful to Shinsei Shigen Kyokai for the financial support.

## References

1) J. C. Maxwell: "A Treatise on Electricity and Magnetism" (Oxford University Press. Oxford. 1891) p. 452.
2) T. Tanaka, S. Hayashi and K. Shibayama: J. Appl. Phys. 48 (1977) 3478.
3) T. Tanaka, S. Hayashi, S. Hirabayashi and K. Shibayama: J. Appl. Phys. 49 (1978) 2490.
4) T. Shimizu: The Research Report of Chubu Electric Power Company, Inc. Electric Lab Ⅱ. 95 (1984) 1.
5) H. Tochiku: National Convention IEE Japan (1983) No. 1293.
6) K. Iwakura: Polymer Preprints Japan 31 (1983) 882.
7) K. H. Stark & C. G. Garton: Nature 176 (1955) 1225.
8) M. Ieda, M. Kosaki & U. Shinohara: J. Phys. Soc. Jap. 18 (1963) 1103.
9) S. Nakamura: Doctor Dissertation (Nagoya University, Japan, 1976).
10) Y. Suzuoki: Doctor Dissertation (Nagoya University, Japan, 1978).
11) Bucci, R. Fieschi & G. Guidi: Phys. Rev. 148 (1966) 816.
12) T. Hino: IEEE Trans. on Electrical Insulation EI-15 (1980) 301.
13) H. F. Mark: Makromol. Chem. 35A (1960) 49.
14) Kosaka: Polymers 18 (1969) 310.
15) M. Yoda: Doctor Dissertation (Nagoya University, Japan, 1975).
16) G. M. Sessler: "Electrets" (Springer-Verlag, Berlin, 1980).
17) J. van Turnhout: "Thermally Stimulated Discharge of Polymer Electrets" (Elsevier, Amsterdam, 1975).
18) M. Dole: "The Radiation Chemistry of Macromolecules" (Academic Press, New York, 1962) vol. 1, p. 193.
19) P. Bräunlich: "Thermally Stimulated Relaxation in Solids" (Springer Verlag, Berlin, 1979).
20) M. Ieda, Y. Suzuoki and T. Mizutani: Kobunshi Ronbunshu 36 (1979) 671.

21) H. A. Flocke: Kolloid-Z. 180 (1962) 118.
22) M. Yoda: Doctor Dissertation (Nagoya University 1975) 76.
23) Fujiki, Uemura and Kosaka: Toyo Soda Kenkyu Hokoku 12 (1968) 24.
24) W. J. Macknight and R. J. Tetreault: J. Polymer Sci. C35 (1971) 117.
25) Y. Inuishi, T. Nakashima, K. Kawabe and M. Ieda: "Yudentai Genshoron" (Dielectric Phenomena) (Denki Gakkai, Tokyo, 1981) p. 112.
26) Y. Suzuoki, G. Cai, T. Mizutani and M. Ieda: Japan. J. Appl. Phys. 21 (1982) 1759.
27) J. Frenkel: Phys. Rev. 54 (1938) 647.
28) M. P. Eidel'nant, F. I. Duntov, V. Kh. Krundel and B. I. Sazhin: Polym. Sci. USSR A15 (1973) 601.
29) Y. Suzuoki, K. Yasuda, T. Mizutani and M. Ieda: Jpn. J. Appl. Phys. 17 (1978) 1215.
30) M. Ieda: "Gendai Kodenatsu Kogaku" (Contemporary High Voltage Engineering) (OHM Publications, Japan, 1981) p. 46.
31) T. Mizutani, Y. Suzuoki and M. Ieda: J. Appl. Phys. 48 (1977) 2408.
32) M. Ieda: "Gendai Kodenatsu Kogaku" (Contemporary High Voltage Engineering) (OHM Publications, Japan, 1981) p. 47.
33) T. Mizutani and M. Ieda: J. Phys. D 12 (1979) 291.
34) M. Ieda, Y. Takai and T. Mizutani: Memoirs of the Faculty of Engineering, Nagoya University 29 (1977) 1.
35) T. Mizutani, Y. Takai and Ieda. M: Trans. I. E. E. Jpn. 48-A40 (1973) 290.
36) K. Yahagi: J. Appl. Phys 37 (1966) 310.
37) M. Ieda, G. Sawa and U. Shinohara: Trans. I. E. E. Jpn. 88 (1968) 163.
38) CRC Handbook of Chemistry and Physics (CRC Press, 1980, Boca Raton) p. E-82.
39) Y. Suzuoki, H. Muto, G. Cai, T. Mizutani and M. Ieda: Jpn. J. Appl. Phys. 23 (1984) 91.
40) B. Hamilton and A. C. Rose-Innes: J. Electrostat. 12 (1982) 121.
41) J Lowell: J. Phys. D: Appl. Phys. 12 (1979) 2217.
42) D. A. Hays: J. Chem. Phys. 61 (1974) 1455.
43) M. Yumoto, T. Takada, T. Sakai and Y. Toriyama: Trans. IEE Jpn. 95-A (1975) 111.
44) E. A. Baum, T. J. Lewis and R. Toomer: J. Phys. D: Appl. Phys. 10 (1977) 487 and 2525.
45) M. M. Perlman K. J. Kao and S Bamji: "Charge Storage, Charge Transport and Electrostatics with Their Applications" (Kodansha Ltd, Tokyo, 1979) p. 3.
46) T. Mizutani, K. Mitani and M. Ieda: Jpn. J. Appl. Phys. 22 (83) 677.
47) T. J. Lewis, R. Toomen and C. Barnes: J. Electrostat 12 (83) 459.
48) T. Mizutani, M. Ieda, S. Ochiai and M. Ito: J. Electrostat. 12 (1982) 427.
49) J. van Turnhout: "Electrets" (Topics in Applied Physics, Vol. 33, Springer-Verlag, Berlin, 1980) ed. G. M. Sessler, 110.
50) G. M. Sessler, J. E. West, D. A. Berkley and G. Morgentern: Phys. Rev. Lett. 38 (1977) 365.
51) P. Laurenceau, G. Dreyfus and J. Lewiner: Phys. Rev. Lett. 38 (1977) 46.
52) R. E. Collins: Rev. Sci. Instrm. 48 (1977) 83.
53) D. E. Cooper: 1977 Annual Report Conference on Electrical Insulation and Dielectric Phenomena (NAS, Washington D. C., 1977).
54) K. P. Homewood: J. Phys. D: Appl. Phys, 17 (1984) 1255-1263.
55) T. J. Fabish, H. M. Saltsburg and M. L. Hair: J. Appl. Phys. 47 (1976) 940.
56) H. Bauser: Dechema Monogr **72** (1974) 11.
57) D. K. Davies: J. Phys. D: Appl. Phys. 2 (1969) 1533.
58) J. Lowell: J. Phys. D: Appl. Phys. 9 (1976) 1571.
59) Lowell and A. C. Rose-Innes: Phys. 29 (1980) 947.